THE BOEING COMPANY
Aerospace Group

# IDENTIFYING OPTIMUM PARAMETERS OF HOT EXTRUSIONS

Contract NAS 7-276

Prepared for

Chief, Materials Research Branch
National Aeronautics & Space Administration
Headquarters
Washington, D.C.

GPO PRICE $ _____

CFSTI PRICE(S) $ _____

Hard copy (HC) 3.00

Microfiche (MF) .65

ff 653 July 65

Progress Report No. 11
11 October 1966 to 11 January 1967

N67 18053
(ACCESSION NUMBER)
44
(PAGES)
CR-81552
(NASA CR OR TMX OR AD NUMBER)
(THRU)
1
(CODE)
15
(CATEGORY)
FACILITY FORM 602

THE BOEING COMPANY
Aerospace Group

# IDENTIFYING OPTIMUM PARAMETERS OF HOT EXTRUSIONS

Contract NAS 7-276

Prepared for

Chief, Materials Research Branch
National Aeronautics & Space Administration
Headquarters
Washington, D.C.

Progress Report No. 11
11 October 1966 to 11 January 1967

## ABSTRACT

Several sets of canned ceramic billets were successfully extruded. Variations in the shape or placement of these billets relative to the extrusion axis, as well as the use of MgO as components of the can, all indicate considerable versatility in the shapes of ceramic bodies that can be extruded. Analysis of these billets is consistent with previous observations and supports the hypothesis that thermal stress is more important than surface shear in causing cracking. Further success in reducing cracking was achieved by again slowing cooling and by use of smaller billets.

Initial comparison shows that starting orientation has little or no effect on extruded orientation.

The successful extrusion of an insulating can consisting of alternate tungsten and MgO layers with MgO billets indicates that extrusion heating temperature may be lowered to reduce grain size, thus further increasing strength. This extrusion was also instrumented with thermocouples which indicate that previous measurements based on optical readings at the rear of the can may be low by 100°C or more. This would explain difficulties observed in recent extrusions and the odd behavior of $Al_2O_3$ extrusions.

CONTENTS


| | Page |
|---|---|
| I. WORK ACCOMPLISHED | 1 |
| A. Billet Preparation | 1 |
| B. Extrusion | 2 |
| C. Material Analysis | 3 |
| II. DISCUSSION | 7 |
| A. Extrusion Temperature | 7 |
| B. Extrusion | 8 |
| C. Extrusion Microstructure | 10 |
| III. SUMMARY AND CONCLUSIONS | 11 |
| IV. FUTURE WORK | 12 |
| APPENDIX 1 | 36 |
| APPENDIX 2 | 37 |
| APPENDIX 3 | 38 |
| APPENDIX 4 | 39 |
| REFERENCES | 42 |

LIST OF FIGURES


| FIGURE | | Page |
|---|---|---|
| 1 | OFF-SET BILLET EXTRUSION CONFIGURATION | 21 |
| 2 | EXTRUSION MgO-18 | 22 |
| 3 | EXTRUSION MgO-19 | 23 |
| 4 | SPLIT CAN WITH A SLOTTED SHELL CONFIGURATION | 24 |
| 5 | INSULATING CAN CONFIGURATION | 25 |
| 6 | TEMPERATURE READING FROM THE INSULATING CAN | 26 |
| 7 | EXTRUSION MgO-21 | 27 |
| 8 | EXTRUSION $Al_2O_3$-3 SAMPLES | 29 |
| 9 | SAMPLE EXTRUSION CROSS SECTIONS | 30 |
| 10 | CROSS SECTIONS OF STALLED JPL HIGH PURITY MgO BILLET | 32 |
| 11 | CRACKING OF STALLED BILLETS | 33 |
| 12 | HAIR LINE CRACKS IN EXTRUDED MgO | 34 |
| 13 | EXTRUDED RUBY MICROSTRUCTURE | 35 |

## LIST OF TABLES


| TABLE | | Page |
|---|---|---|
| I | BILLET FABRICATION | 14 |
| II | EXTRUSION PARAMETERS | 17 |
| III | EXTRUDED BILLET DATA | 18 |
| IV | BILLET GRAIN SIZE AFTER HEATING FOR EXTRUSION | 20 |

## I. WORK ACCOMPLISHED

### A. Billet Preparation

MgO and MgO alloy billets were vacuum hot pressed per Appendix 1, except for temperatures of applying and holding pressure which are shown in Table I along with firing temperatures and results. Mallinckrodt MgO densifies in the center first, leaving a somewhat porous outer shell. This lower density outer shell is reflected in the slightly lower densities shown in Table I for this material.

An attempt to vacuum hot press a MgO-5 w/o NiO billet of theoretical density at 10,000 psi (in order to keep temperatures low enough to limit decomposition of NiO-see Table I) was unsuccessful due to die failure. However, a large fragment had a density of 3.63 gm/cc indicating the right range of parameters for improved density in this composition.

$Al_2O_3$ billets were vacuum hot pressed per Appendix 1, except for temperatures of applying and holding pressure which are shown in Table I along with firing temperature and results.

CaO, calcined from reagent grade $Ca(OH)_2$ per Appendix 2, was vacuum hot pressed at about one-half the heating rate for MgO (Appendix 1). The temperatures and times are shown in Table I along with firing temperatures and results. Two billets, which had been previously partially vacuum hot pressed, were subsequently vacuum hot pressed together with some CaO + 2 w/o LiF powder between them. Good bonding was indicated, but densification (Table I) was not complete indicating that temperature, time or pressure were a little low.

Other $Al_2O_3$ billets were cut from 1" diameter commercial rods as shown in Table I.

Spinel* (approximately 3 MgO to 3.5 $Al_2O_3$), and ruby** billets were cut from single crystal boules by diamond sawing and tool post grinding. MgO billets consisting of all or part of two or more crystals were similarly cut from fused MgO as shown in Table I.

Two hot pressed MgO billets, one of Fisher MgO and one of high purity MgO developed at the Jet Propulsion Laboratory, designated respectively OP-211 and OP-225 were received***.

*Purchased from Hrand. Djevaihrdjian S.A., Monthey, Switzerland.
**Purchased from Grieger's, Pasadena, California.
***Courtesy of M. Leipold of the Jet Propulsion Laboratory (herein designed JPL).

Some pure MgO powder produced by the Kanto Chemical Company of Japan was received*.

B. Extrusion

Because of the possible melting of earlier $Al_2O_3$ extrusions, an empty tungsten can was heated in the furnace and optical sightings were taken on the rear of the can and the inside of the nose. These were in good agreement and the can appeared to be uniformly heated.

Extrusion parameters for all recently run extrusions are shown in Table II, and the billets used and their order are shown in Table III.

Extrusions MgO-18 and -19 both extruded as planned, producing continuous rods which were brought to rest in the heated catch tube by leaving the tail unextruded. MgO-18 consisted of square billets, some of which were selectively oriented single crystals. MgO-19 contained billets of different diameters, with some off-set from the can axis as shown in Figure 1. In both cases tungsten pieces to fit the square or off-set billets to a single cylindrical cavity on the can axis were machined from tungsten powder cold pressed to about 90% theoretical density at about 90 tons/in$^2$ in a rubber mold in a blanked-off extrusion press. In extrusion MgO-19 some sintered tungsten pieces were used as shown in Figure 1. The resultant extrusions are shown in Figures 2 and 3. Extrusion MgO-19 was accidently broken in several pieces while being radiographed.

The third $Al_2O_3$ extrusion was run next. As extrusion started, about a 1-foot section of the nose shot out of the press and through the heated catch tube breaking the graphite end seal and quartz window. The extrusion was stopped with about 70% extrusion by the press operator in response to this unexpected pyrotechnic display. No fire or serious damage to the catch tube resulted.

The next attempted extrusion, MgO-20, involved a slotted TZM shell over a split tungsten can (from earlier work - see Figure 4). This failed to drop from the furnace when released. After cooling it was found that about the central third of the TZM shell had melted. The tungsten can and billets appear salvageable.

*Courtesy of W. Sibley of Oak Ridge National Laboratory.

The insulating can extrusion*, MgO-21, utilized sintered tungsten sleeves and MgO grain sleeves (Figure 5). (A previous attempt, using tungsten grain sleeves and sintered MgO sleeves, failed due to melting of the TZM shell in a graphite susceptor furnace). In order to check both the internal heating of the can and the uniformity of the furnace, two tungsten-5% rhenium, tungsten-26% rhenium couples in single hole MgO insulators were placed in the MgO shells about half way between front and rear (see Figure 5). The relative temperatures of these and the optical readings at the rear of the can are shown in Figure 6. The extrusion was dropped at an optical reading of 2080°C. The composite can and billets were successfully extruded (without the catch tube to test for its insulation ability after extrusion). The extrusion broke into 8 pieces, the shortest of which was about 6" and the longest about 24" (see Figure 7A). Of the 7 breaks, 5 were at or near the termination of the ceramic billets, and the other 2 appeared to be at or near junctions of the tungsten sleeves. In several cases the breaks occurred where the outer extruded TZM shell had separated over about 1" of length.

C. Material Analysis

(1) Extrusion Uniformity

The $Al_2O_3$ extrusion ($Al_2O_3$-3) was extremely non-uniform with much of the material occurring in "lumps" along the rod (e.g. see Figure 8). Most of the material appeared to be in the front half of the can. Some material which appeared to have melted and flowed out of the break in the can was also found. The spinel had partially extruded around and in front of the ruby as shown in Figure 8.

The square billets extruded through a round die (in a round can, extrusion MgO-18), were quite uniform as shown in Figure 2. This is also shown by less variation in reduction ratio in Table III. All of the noses were round, and some were slightly bulbous; however, these rapidly became fairly uniform reductions of the original square cross section (see Figure 9).

The extrusion with billets off-set from the axis (MgO-19) was fairly uniform (see Figure 3E, F). The greatest non-uniformities were in billets around which pressed tungsten powder rather than sintered tungsten was used as spacers between the billets and the can (see Figure 3). The extreme of this was in the off-set billets shown in Figure 9C, D.

*The concept is to provide insulating layers and interfaces in the can to reduce heat loss. This should reduce the initial heating required by reducing losses during billet loading and reduce cracking on cooling. Excessive cooling is expected to be reduced by shattering of the ceramic insulating layers. MgO is chosen because of its established compatibility and extrudability with tungsten.

The MgO billets in the insulating can extrusion (MgO-21) extruded as uniformly as in other extrusion (see Figures 7 and 9). However, the MgO-5 w/o NiO was rather non-uniform as shown in Figure 9-I and -J).

(2) Can Bonding and Reaction

No discoloration, bonding to the can, or other sign of reaction was observed between the tungsten and hot pressed MgO in the stalled square die extrusion (MgO-17). The powder billet appeared to have some discoloration.

The square extruded billets of extrusion MgO-18 all showed some sign of being affected by the pressed tungsten in contact with them. The three fused MgO crystals showed only a frosting of the surface but no sign of coating or contamination. All other billets showed some bonding, discoloration, or both (Figure 2). The MgO-5 w/o NiO billet (M5N-1-9), which was black except for a small central region of green, was tightly bonded as was the preceeding MgO billet (M-3-28). All hot pressed MgO billets showed a gray-green discoloration, especially the last one (M-3-29) around the TZM tail plug. The MgO-1 w/o $Al_2O_3$ billet (M1A-1-12) was the least affected of the hot pressed billets.

Some of the billets in extrusion MgO-19 showed some discoloration though not near as severe as above, and some did not. The worst were those in contact with the pressed tungsten powder and some of these appeared affected only in the outer half. Those not showing signs of discoloration were not in contact with tungsten and generally not close to it. OP-225 (unfired hot pressed Fisher MgO from M. Leipold at JPL) had a blue color over the central half of the cross section in some pieces. No bonding was observed.

Little or no discoloration occurred in the hot pressed or fused billets in the insulating can extrusion (MgO-21), except for a small black rim around the outside of the otherwise green MgO-5 w/o NiO billet (M5N-1-10). No obvious discoloration occurred in the fused MgO grain used for insulating layers. The "powder" billets showed some definite discoloration, especially the Kanto MgO (m-2-1). A slight sign of bonding to the can was seen with the Kanto MgO. Some of the MgO insulating grain, which extruded to a dense coating, showed some bonding. However, this appeared associated with mechanical gripping due to some conformation of the can around the larger original grains (see Figure 7-B and -C). Limited mechanical forcing always removed this MgO through its complete

thickness leaving a bright metallic surface on the metal and no sign of contamination on the MgO. Even the tungsten foil around the hot pressed MgO and MgO-1 w/o $Al_2O_3$ billets was a thin bright layer that was readily peeled off of the billets when the outer "insulating" MgO was removed. In the case of the MgO powder, and the hot pressed MgO-5 w/o NiO billets, the tungsten foil had a bright metallic appearance on the outside, but was bonded to the billets.

Examination of the spinel and ruby in the $Al_2O_3$ extrusion showed the former to be translucent white, and the latter transparent pink indicating that little or no reduction or contamination had occurred.

(3) Density

Transparency and translucency in the ruby and spinel respectively indicates that little or no porosity had been introduced (extrusion $Al_2O_3$-3).

Examination of the stalled hot pressed Fisher MgO billets from extrusion MgO-17 showed all were fairly translucent, except for cracking, which indicates near theoretical density. The Fisher MgO powder billet, m-1-4, was almost as translucent as the hot pressed billets, indicating substantial densification from its original cold pressed state. The outer rim of the high purity JPL MgO (OP-211) was glass clear, while the center was nearly opaque (see Figure 10) indicating a varying density.

Density data for several of the extruded billets is shown in Table III. All hot pressed billets in contact with the pressed tungsten were opaque, at least in the outer half, indicating a reduction in density. This was particularly pronounced in extrusion MgO-18, except for the MgO-1 w/o $Al_2O_3$ billet which was affected less.

All hot pressed and powder billets in the insulating can extrusion (MgO-21) densified some, based on observations of transparency and density measurements. The least dense billets densified most, but the denest starting billets produced the densest extruded billets. The Mallinckrodt MgO billet (M-4-11), which was porous in the outer half before extrusion, was uniformly translucent to transparent across the entire cross section after extrusion.

(4) Cracking

The stalled Fisher MgO billets of extrusion MgO-17 all had some cracks like those in Figure 11. However, the high purity JPL MgO showed a different pattern as seen in Figure 10. Many, and possibly all of the radial lines of the perimeter appear to be cracks. The nearly opaque interior has a few hair line cracks.

All extruded fused billets had longitudinal cracking (i.e. cracks parallel to the extrusion axis) which appeared to follow the remnants of original grain boundaries of the columnar grains (Figure 9A).

Transverse cracking in the fused billets of extrusion MgO-18 was exclusively cleavage. These cracks appeared to originate from two or more locations along the original longitudinal grain boundaries. Several sections 1" to 2" in length were free of transverse cracks in these fused, square billets (see Figure 2). The hot pressed billets of this extrusion had similarly spaced transverse cracks (Figure 2); however, the intervening sections had a high density of hair line cracks as shown in Figure 12. Distinct longitudinal cracking in these hot pressed billets appeared to be only in the MgO-1 w/o $Al_2O_3$ billet (M1A-1-12).

In extrusion MgO-19, transverse cracking was by far the most frequent in billets in contact with the pressed tungsten powder (see Figure 3). Numerous hair line cracks occurred in at least the outer portion of these and adjacent billets. All transverse fracturing in billets without discoloration or hair line cracks were exclusively cleavage, while much of the transverse cracking of billets with discoloration and hair line cracks appeared to be intergranular. Longitudinal cracks were few, and appeared limited to central sections of the largest (0.5" diameter) extruded pieces. No asymmetry of cracks was observed in the off-set billets. Of particular note is the very limited cracking of billets originally 1" in diameter located on the can axis. Sections from over 1" to nearly 6" in length appear to be crack free.

At the place where the nose of the $Al_2O_3$ extrusion broke off, the ruby shows planar, parallel cracks (Figure 8B) inclined at about 30° to the extrusion, and as-grown ruby boule axis. These appeared to be extensions of some of the lines of Figure 13. Figure 13-A also shows some much smaller perpendicular cracks.

No obvious longitudinal cracking was observed in the insulating can extrusion, except for a few possible ones in the MgO-5 w/o NiO body. Transverse cracks were spaced about 0.25 to about 1.0" apart. It was exclusively cleavage in all dense bodies, and about half or more cleavage in the less dense powder billets. The MgO grain insulation had many hair line cracks as shown in Figure 7C, but showed no sign of continuous circumferential separation.

(5) Microstructure

Grain sizes of the stalled billets of extrusion MgO-17, along with grain sizes from some earlier stalled billets are given in Table IV. Of particular

note, is that the perimeter and front end of the high purity JPL MgO appears to consist of very clear, extremely large (about 3000 microns) grains (see also Figure 10). Most of the apparent cracking in this region appears to be along the grain boundaries. The nearly opaque interior has about 1/30th of this grain size.

Sample microstructural data of extruded MgO and MgO alloy bodies is shown in Table III.

Examination of the spinel ring around the ruby (see Figure 8) showed an apparently radially oriented columnar grain structure. The ruby on the other hand, as previously noted had many fine laminar layers spaced from less than 10 to over 100 microns apart. Some of these were slightly bent (see Figure 13A). These laminar layers appeared to occur in sections about 1000 microns in size, which sometimes had markedly different laminar orientations. (Figure 13B).

## II. DISCUSSION

### A. Extrusion Temperature

All previous extrusion heating temperatures have been measured optically at the rear of the billet. Comparison of the thermocouple and optical data of Figure 6 shows that the latter can be low by 100°C or more, depending on heating rate and soak time, in the temperature range commonly used for extrusion. Increasing heating rate or decreasing soak time would be expected to increase this differential. (Normal heating has previously taken about 15 minutes, about 12 minutes at 60KW then dropping to 35KW, followed by a 5 minute soak for equilibrium).

This differential may explain the melting of the $ZrO_2$ refractory furnace lining reported in Progress Report No. 10, since the optical temperature at the can rear was 2400°C, which could put some areas of the tungsten can, which is only about 0.1 inch from the refractory, above the expected refractory melting range of 2600-2700°C. Similarly, this differential may explain the melting of the TZM shell on the attempted high reduction extrusion (MgO-20) with an optical reading of 2200°C. The slots in this TZM shell may have also contributed to the melting by concentrating heating in that region. This differential would also suggest that melting occurred in all three $Al_2O_3$ extrusions, explaining their odd behavior. This is also supported by direct observations indicating melting in this last $Al_2O_3$ extrusion.

The melting of the $ZrO_2$ refractory and the TZM can occurred in about the center third of the can indicating a lower nose as well as a lower tail temperature. This would explain why the front $Al_2O_3$ billet in the first $Al_2O_3$ extrusion behaved normally. Being cooler, it would not have melted, or could have solidified first, thus extruding as a solid and not a fluid. This also appears to be the case in the latest $Al_2O_3$ extrusion where the angular shape of the ruby (Figure 13) and the extrusion of the spinel around it suggest that the ruby did not melt.

Two factors could explain the failure to detect such a gradient with optical readings in the heated empty tungsten can. First, since the can was empty, it would allow interchange of radiation between the walls which may bring the can closer to equilibrium, and would make optical measurements inside appear uniform. Second, the apparent gradient both toward the front and rear would make the nose and rear readings similar as observed.

This apparent temperature measurement problem is believed to be restricted primarily to extrusions in this year's study with the new $ZrO_2$ induction furnace built to accommodate longer billets and to prevent Mo-C or W-C eutectics. It may have been a factor in the Mo-C eutectic melting of canning materials in the graphite susceptor furnace used for longer billets during the latter part of last year's study. However, any such effects would be expected to have been reduced by the use of a susceptor longer than the cans. Extrusions in approximately the first year and a half should have been least affected because shorter billets were used. Reduction of billets with NiO (as indicated by blackening) tends to support this (e.g. over half of the outer material in the square MgO-NiO body was black, but only a very thin layer of a similar body in the insulating can was black).

B. Extrusion

The successful coextrusion of the alternate metal and ceramic layers in the insulating can extrusion is a significant demonstration of the compatibility and co-extrudability of TZM, tungsten, and MgO. Use of continuous metal sleeves, and a solid metal sleeve in contact with the MgO should reduce breakage of the can since such breakage was usually associated with junctions between billets or sleeve segments. The successful extrusion of the square and off-set billets with reasonable to excellent maintenance of shape also shows this co-extrudability and indicates that considerable versatility of shape of ceramic extrusions is feasible.

The discoloration of MgO billets in contact with the pressed tungsten powder indicates some incompatibility. This is probably due to trapped oxygen producing $WO_3$ during heating. The apparent excess heating in these extrusions

may have accentuated this problem. However, it appears to be a basic problem since billets in contact with the pressed tungsten powder in the apparently cooler nose also showed signs of degradation, while those billets in contact with the sintered tungsten that were also probably over heated showed no such problem. The surface frosting of the square fused billets in contact with the pressed tungsten appears to be due to microscopic surface roughness probably arising from the initial porosity of the pressed tungsten. The lack of effects other than frosting in the fused MgO shows that the degradation in hot pressed MgO must be due to grain boundaries, small amounts of porosity, or contaminants in the hot pressed bodies.

The hair line cracking and increased transverse cracking in the hot pressed billets in contact with the pressed tungsten powder are probably due to gripping of the ceramic by the can resulting from both macroscopic and microscopic surface roughness. Greater strength of the hot pressed material and subsequent contamination may have also increased this cracking.

The hypothesis of cracking being partially due to mechanical gripping is also supported by the surface roughness and fine cracking in the extruded MgO grain insulation of the insulating can extrusion. Similarly, transverse cracking of the billets in this extrusion may have been increased due to surface roughness from the MgO grain penetrating through the tungsten foil from the surrounding MgO grain. Use of a solid sleeve around the MgO should reduce this.

Thermal stress or surface shear have been shown in previous work to be an additional cause, and probably the major cause, of transverse cracking. Evidence has favored thermal stress over shear. If shear, which goes from zero at the center to a maximum at the surface, were the primary cause of this cracking, one would have expected more or bigger transverse cracks in the outside of the off-set billets and in the outer MgO grain insulation layers. Since (1) transverse cracking of the off-set billets was about the same as comparable billets on the extrusion axis and was not asymmetrical, and (2) only uniform, hair line cracking was observed in all MgO grain layers; evidence again favors thermal stress over surface shear.

No difference was seen in initial observations of the fracture of the three square MgO crystal (fused) billets. Fracture has been a good indication of orientation, and the three starting crystals were of different orientation ( $\langle 100 \rangle$ , $\langle 110 \rangle$ , $\langle 111 \rangle$ ). Thus, there appears to be little or no effect of initial orientation on extruded orientation.

This further analysis on the cause of cracking should not obscure the progress in reducing and eliminating cracking. The square fused billets (extrusion MgO-18) had substantially less than average cracking due to either their

smaller cross section or the heated catch tube. The latter appears to be the reason for reduction of longitudinal and possibly transverse cracking in 1.5" diameter starting billets in extrusion MgO-19 despite possible complications due to proximity to pressed tungsten powder sleeves. This latter extrusion again demonstrates the attainment of essentially crack free extrusions using 1" diameter billets in a 3" diameter tungsten can extruded at 9 to 1 area reduction ratio without slowed cooling since:

(1) Pieces up to 6" long, apparently free of cracks, were obtained in both the front and back of the extrusion. The back is not in the catch tube because it is stalled in the die to bring the front portion to rest in the hot zone of the catch tube.

(2) Most, if not all of the cracking in these billets is believed to have been caused by the accidental breaking of this extrusion.

The reduction or elimination of longitudinal cracking as well as the comparable or reduced transverse cracking despite apparent mechanical gripping (which can be substantially reduced) in the insulating can extrusion is also very encouraging.

C. Extrusion Microstructure

This work has further reinforced earlier observations that:

(1) The largest starting grain size undergoes the greatest reduction in grain size, but the finest starting grain size will produce the finest extruded grain size if comparable densities also occur.

(2) The least dense billets undergo the greatest densification, but the highest starting density generally results in the highest extruded density.

(3) Longitudinal fused grain boundaries generally result in longitudinal cracks after extrusion.

In conjunction with this latter point, it is also noted that apparent origins of transverse fracture observed at these boundaries indicates that they also did transverse fracturing.

The marked surface grain growth of the high purity JPL MgO is probably due to its greater purity and is consistent with Leipold's observation of higher grain growth in this material. The gradient in grain size is probably due to thermal gradients during heating; however, the very abrupt change in the grain size and transparency seems somewhat surprising. This could be due to gas from

impurities (as discussed in the Appendix of Progress Report No. 10) such as $Mg(OH)_2$ and $MgCO_3$ being released from near the surface, but getting trapped in the center. The apparent radial cracks, which often seem to follow grain boundaries may have resulted in part from the release of such gases from the center. The release of such impurities may have contributed to this radial grain growth in the high purity JPL MgO and not have been all caused directly from growth in a thermal gradient. This would be in agreement with the fact that the heated Boeing Fisher MgO, which was previously fired to reduce such contaminants, had no obvious grain size gradient although being larger may have had a much greater thermal gradient which could compensate some for its slower grain growth rate.

The extremely high grain growth shown in this pure MgO indicates the need for alloying to control grain growth. (The blue central discoloration of the JPL Fisher MgO may also be due to gas producing impurities since this billet was not previously fired).

In the Second Interim Report and Progress Report No. 10, evidence was presented showing that mechanical preparation of extruded MgO work hardens surface grains. Sample observations on similar preparation of MgO crystals lends further support to this hypothesis and previous observations (see Appendix 4).

The lamellae in the extruded ruby are probably twins. The irregular, angular shape of the ruby may in part represent the resistance of $Al_2O_3$ to deformation rather than being due entirely to melting of other bodies in the extrusion.

## III. SUMMARY AND CONCLUSIONS

A temperature drop of about 100°C or more from the center to the front and rear of the cans is indicated. This would explain difficulties recently experienced in several extrusions and the odd behavior in the $Al_2O_3$ extrusion attempts. The extrudability of $Al_2O_3$ appears to be confirmed based on normal extrusion behavior in the nose of a previous $Al_2O_3$ extrusion which had no melting. Substantial twinning appears to occur in extruded ruby.

Considerable versatility of extruded MgO shapes has been shown feasible.

Starting crystal orientation appears to have little or no effect on extruded orientation.

The insulating can configuration was successfully extruded and indicates that the concept of slower cooling may be working to reduce cracking.

Cracking again appears to have been reduced by use of smaller billets and by use of the heated catch tube.

Further evidence of the following phenomena, previously observed, have been found:

1. The decreasing importance respectively of thermal stress, mechanical gripping, and surface shear in causing cracking.

2. That transverse and longitudinal cracking are not caused by the same parameters.

3. That original fused boundaries cause cracking, much of it along the boundary, after extrusion.

4. The largest grain size undergoes the greatest reduction, but the finest starting grain size generally results in the finest extruded grain size.

5. The least dense starting billet undergoes the greatest densification, but the densest starting body generally produces the densest extruded body.

6. That mechanical preparation of MgO surfaces results in surface work hardening.

7. That gas producing impurities are a problem in hot pressed billets.

8. That powder billets generally result in less dense and more contaminated bodies.

## V. FUTURE WORK

Several of the billets in the extrusions discussed in this report have finer than average grain sizes which will be useful for room and elevated temperature testing. Of particular interest for elevated temperature testing are the finer grain extruded fused MgO bodies since these should not be affected by gas producing impurities. Also, the lack of longitudinal cracking, especially in the insulating can extrusion, will provide more testing with fracture parallel with the extrusion axis. Such further mechanical testing will be done.

Further evaluation of temperature errors and necessary corrections and adjustments will be made.

The second square die and alloy extrusion attempts will be run and analyzed with high priority because of their possible contribution toward increased strength by changing texture and controlling grain size respectively.

Another insulating can extrusion will be run now that the configuration has been shown to extrude successfully. The temperature will be lowered about 100°C to

test the main function of this concept: namely, obtaining finer grain sizes by requiring less heating due to reduced heat loss during transfer of the hot billet to the extrusion press. More TZM will be used at the lower temperature. Continuous metal sleeves, one being around the MgO will be used. A design using MgO "insulation" that may also provide test specimens will be considered.

Another $Al_2O_3$ extrusion will be run with melting eliminated.

TABLE I - BILLET FABRICATION

| Billet | | | Pressing[1] | | | | |
|---|---|---|---|---|---|---|---|
| Number | Composition | Diameter (inches) | Pressure Applied at: | Held at: | For (min): | Fired to:[2] | Density[3] gm/cc |
| M-4-1 | Fisher MgO | 1.0 | 2400°F(1315°C) | 2400°F(1315°C) | 15 | 2200°F(1205°C) | 3.59 |
| M-4-2 | | 1.0 | | | 10 | | 3.56 |
| M-4-3 | | 1.0 | | | 15 | | 3.59 |
| M-4-4 | | 1.0 | | | | | 3.58 |
| M-4-5 | | 1.0 | | | | | 3.58 |
| M-4-6 | | 1.0 | 2400°F(1315°C) | | | 2200°F(1205°C) | 3.59 |
| M-4-7 | Fisher MgO | 1.5 | 2350°F(1285°C) | | | 2850°F(1565°C) | 3.58 |
| M-4-8 | Mallinckrodt MgO | 1.5 | | | | 2850°F(1565°C) | 3.52 |
| M-4-9 | Fisher MgO | 1.5 | | | | 2600°F(1425°C) | 3.59 |
| M-4-10 | Mallinckrodt MgO | 1.5 | | | | | 3.54 |
| M-4-11 | Mallinckrodt MgO | 1.5 | | | | | 3.53 |
| M-4-12 | Fisher MgO | 1.0 | 2350°F(1285°C) | | | | 3.58 |
| M-4-13 | Mallinckrodt MgO | 1.0 | 2380°F(1305°C) | | | | 3.54 |
| M-4-14 | Fisher MgO | 1.0 | 2370°F(1300°C) | 2400°F(1315°C) | | | 3.58 |
| M-4-15 | Mallinckrodt MgO | 1.0 | 2350°F(1285°C) | 2410°F(1320°C) | | 2600°F(1425°C) | 3.56 |
| M-4-16 | Fisher MgO | 1.5 | 2380°F(1305°C) | 2400°F(1315°C) | | | 3.58 |
| M-4-17 | Fisher MgO | 2.0 | 2400°F(1315°C) | 2400°F(1315°C) | 15 | | |
| M-f-13 | Fused Norton MgO Crystals | 1.25 | | | | | |
| M-f-14 | | 1.1 | | | | | |
| M-f-15 | | 0.9 | | | | | |
| M-f-16 | | 1.2 | | | | | |
| M5N-1-12 | MgO + 2 w/o NiO | 1.5 | 2140°F[4](1170°C) | 2290°F(1255°C) | 11 | Die Broke | |
| M1C-1-4 | Fisher MgO + 1 w/o CaO | 1.0 | 2350°F(1285°C) | 2400°F(1315°C) | 15 | 2600°F(1425°C) | 3.57 |
| M1C-1-5 | | 1.0 | 2350°F(1285°C) | 2400°F(1315°C) | 15 | 2600°F(1425°C) | 3.57 |

TABLE I - (CONT'D)

| Billet | | | Pressing[1] | | | | |
|---|---|---|---|---|---|---|---|
| Number | Composition | Diameter (inches) | Pressure Applied at: | Held at: | For (min): | Fired to:[2] | Density[3] gm/cc |
| M2C-1-4 | Fisher MgO + 2 w/o CaO | 1.0 | 2350°F(1285°C) | 2400°F(1315°C) | 15 | 2600°F(1425°C) | 3.58 |
| M2C-1-5 | | 1.0 | 2350°F(1285°C) | 2400°F(1315°C) | 15 | 2600°F(1425°C) | 3.58 |
| MZ/2-1-4 | MgO + 1/2 w/o $ZrO_2$ | 1.0 | 2380°F(1305°C) | 2400°F(1315°C) | 15 | 2600°F(1425°C) | 3.57 |
| MZ/2-1-5 | | 1.0 | 2400°F(1315°C) | 2400°F(1315°C) | 15 | | |
| A-1-4 | Coors AD99 | 1.0 | | | | | |
| A-1-5 | Linde A $Al_2O_3$ | | 2300°F(1260°C) | 2500°F(1370°C) | 45 | 2650°F(1455°C) | 3.89 |
| A-1-6 | | | 2360°F(1290°C) | 2600°F(1425°C) | 20 | 2650°F(1455°C) | 3.91 |
| A-1-7 | Linde A $Al_2O_3$ | | 2300°F(1260°C) | 2700°F(1480°C) | 30 | 3000°F(1650°C) | 3.87 |
| A-1-8 | Reynolds RC-965[5] | | 2400°F(1315°C)[6] | 2700°F(1480°C) | 15 | 3000°F(1650°C) | 3.88 |
| A-1-9 | Linde A $Al_2O_3$ | | 2400°F(1315°C) | 2700°F(1480°C) | 30 | 2650°F(1455°C) | 3.13 |
| A-1-10 | Morganite Triangle RR Recrystallized $Al_2O_3$ | 1.0 | | | | | |
| A-1-11 | | 1.0 | | | | | |
| A-1-12 | General Electric Lucalox $Al_2O_3$ (+ 0.25 MgO) | 1.0 | | | | | 3.98 |
| A-1-13 | | 1.0 | | | | | |
| A-1-14 | Coors AD 99 | 1.0 | | | | | 3.86 |
| A-1-16 | Ruby Boules | 0.75 | | | | | 4.00 |
| A-1-17 | | | | | | | |
| A-1-18 | | | | | | | |
| C-1-7 | CaO + 2 w/o LiF | 1.5 | Specimen Blew Up | | | | |
| C-1-8 | CaO + 2 w/o LiF | 1.5 | 1700°F(925°C) | 1700°F(925°C) | 5 | | |
| C-1-9 | CaO + 2 w/o LiF | 1.5 | 1700°F(925°C) | 1700°F(925°C) | 5 | | |
| C-1-10 | C-1-8 and -9 hot pressed together - see Text. | 1.5 | 1800°F(980°C) | 1900°F(1040°C) | 15 | 2500°F(1370°F) | 3.04 |

TABLE I - (CONT'D)

| Billet | | | Pressing[1] | | | | |
|---|---|---|---|---|---|---|---|
| Number | Composition | Diameter (inches) | Pressure Applied at: | Held at: | For (min): | Fired to:[2] | Density[3] gm/cc |
| C-1-11 | CaO | 1.0 | 2300°F(1260°C) | 2300°F(1260°C) | 30 | 2650°F(1455°C) | 3.31 |
| C-1-12 | CaO | 1.0 | 2300°F(1260°C) | 2300°F(1260°C) | 30 | 2650°F(1455°C) | 3.21 |
| Sma-2-1<br>Sma-2-1<br>Sma-2-3 | Spinel Crystal Boules | 0.8 | | | | | 3.64 |

(1) Pressed at 5000 psi unless noted otherwise.

(2) On Firing Schedule A (Appendix 3)

(3) After firing (if any). Nominal error ±0.01 gm/cc.

(4) Pressed at 10,000 psi.

(5) Powder courtesy of D.V. Royce, Jr., Director of Basic Research, Alumina Div. of Reynolds Metals Company.

(6) Pressed at 7500 psi.

TABLE II - EXTRUSION PARAMETERS

| Extrusion Number | Can Material | Can Outside Dia. (in) | Ceramic Billet Diameter (in) | Temperature[1] °C | Area Reduction Ratio | Speed in/sec | Forces (tons) Upset[2] | Forces (tons) Running | Catch Tube Temp. Just After Extrusion |
|---|---|---|---|---|---|---|---|---|---|
| $Al_2O_3$-1 | Cold pressed tungsten grain, TZM | 3.5 | 1.0-1.5 | 1950 | 9 to 1 | 15 | 825 | 550 | None |
| $Al_2O_3$-2 | TZM | 3.0 | 1.0-1.5 | 1850 | 9 to 1 | 6.7 | 600 | 600 | 1650°C |
| $Al_2O_3$-3 | TZM | 3.5 | .75-1.0 | 1900 | 9 to 1 | 15 | 800 | 625 | 1700°C |
| MgO-17 (Square Die) | Tungsten | 3.0 | 1.0-2.0 | 2200 | Stalled | | | | |
| MgO-18 (Square billets in round can) | Tungsten | 3.0 | .72 × .83[3] 1.4 × 1.4 | 2200 | 9 to 1 | 2.5 | No data due to recorder manfunction. | | 1750°C |
| MgO-19 (Off-Set Billets) | Tungsten | 3.0 | 1.0-1.5[4] | 2200 | 9 to 1 | 5.0 | 750 | 700 | 1750°C |
| MgO-20 (High reduction ratio) | TZM, Tungsten | 3.5 | 1.5 | Aborted due to melting of TZM. | | | | | |
| MgO-21 (Insulating can) | TZM, MgO,[5] Tungsten | 3.5 | 1.5 | 2080 | 9 to 1 | 15 | 925 | 700 | None |
| MgO-22 (Square Die) | Tungsten | 3.0 | 1.0-1.5 | Not yet extruded. | | | | | |
| MgO-23 | Tungsten | 3.0 | 1.0-1.5 | 2350 | Aborted due to melting of furnace liner. | | | | |

(1) Temperature (measured optically in sight hole in the rear of the can) of composite can-ceramic billet on dropping from furnace.

(2) Force to extrude metal nose.

(3) Length and width.

(4) See Figure 1.

(5) See Figure 5.

## TABLE III - EXTRUDED BILLET DATA

| Number[1] | Composition | Fabrication[2] | Density (gm/cc) Before Extrusion[3] | Density (gm/cc) After Extrusion[4] | Area Reduction Ratio | Average Grain Size (microns) Transverse | Average Grain Size (microns) Longitudinal | Orientation High | Orientation Low | Orientation Avg. |
|---|---|---|---|---|---|---|---|---|---|---|
| (Extrusion MgO-17, Square Die Extrusion, Drop Temperature 2200°C, Area Reduction Ratio: 9 to 1) | | | | | | | | | | |
| OP-211 | MgO | B | 3.58[5] | | | | | | | |
| M-3-11 | MgO | B | 3.59 | | | | | | | |
| M-3-22 | MgO | B | 3.60 | | | | | | | |
| M-3-16 | MgO | B | 3.59 | Stalled, with Ceramic Unextruded. | | | | | | |
| M-3-20 | MgO | B | 3.58 | | | | | | | |
| m-1-4 | MgO | Powder | ~1.5 | | | | | | | |
| M-3-6 | MgO | B | 3.58 | | | | | | | |
| Extrusion MgO-18 (Square Billets Through Round Die), Drop Temperature: 2200°C, Area Reduction Ratio: 9 to 1) | | | | | | | | | | |
| M-f-10 | MgO⟨100⟩ Orient. | Fusion | 3.58[5] | 3.58[5] | 7-8 to 1 | 53 | | | | |
| M-f-11 | MgO⟨110⟩ " | Fusion | 3.58[5] | 3.58[5] | 5-7 to 1 | 37 | | | | |
| M-f-12 | MgO⟨111⟩ " | Fusion | 3.58[5] | 3.58[5] | 7-8 to 1 | 98 | | | | |
| M-3-28 | MgO | B | 3.59 | | 7.5-8.5 to 1 | | | | | |
| M5N-1-9 | MgO+5 w/o NiO | B | 3.54 | | 8-9 to 1 | | | | | |
| M1A-1-12 | MgO+1 w/o $Al_2O_3$ | B | 3.58 | | 7-8 to 1 | 20 | 16 | | | |
| M-3-30 | MgO | B | 3.58 | | 7.5-8.5 to 1 | 32 | 28 | | | |
| M-3-29 | MgO | B | 3.57 | | 7.5-8.5 to 1 | | | | | |
| Extrusion MgO-19 (Billets side-by-side off-set from axis); Drop Temperature: 2200°C, Area Reduction Ratio: 9 to 1) | | | | | | | | | | |
| OP-225 | MgO - from M. Leipold (JPL) | Hot-pressed | 3.58[5] | | 6.5-11.5 to 1 | 26 | | | | |
| M-4-3 | MgO | B | 3.59 | 3.57 | 8-9 to 1 | 36 | | | | |
| M-3-4 | MgO | B | 3.55 | 3.58 | 9-11 to 1 | | | | | |
| M-4-4 side- | MgO see Fig. 1 | B | 3.58 | | 7-9 to 1 | | | | | |
| M-4-5 by- | MgO see Fig. 1 | B | 3.58 | | 6-9 to 1 | 17 | | | | |
| M-4-1 side | MgO see Fig. 1 | B | 3.59 | | 7.5-9.5 to 1 | | | | | |
| M-4-6 " | MgO see Fig. 1 | B | 2.59 | | 7.5-9.5 to 1 | | | | | |
| M-2-4 | MgO | B | 3.58 | 3.58 | 8-9 to 1 | 27 | | | | |
| M-4-2 | MgO | B | 3.56 | 3.57 | 11-12 to 1 | 22 | | | | |
| m-1-5 | MgO | Powder | 1.5 | 3.52 | 22-28 to 1 | 24 | | | | |

TABLE III - (CONT'D)

| Number[1] | Composition | Fabrication[2] | Density (gm/cc) Before Extrusion[3] | Density (gm/cc) After Extrusion[4] | Area Reduction Ratio | Average Grain Size (microns) Transverse | Average Grain Size (microns) Longitudinal | Orientation High | Orientation Low | Orientation Avg. |
|---|---|---|---|---|---|---|---|---|---|---|
| (Extrusion MgO-20 Attempted High Reduction, aborted due to melting of TZM shell) | | | | | | | | | | |
| M-f-8 | MgO | Fusion | 3.58[5] | | | | | | | |
| M-1-17 | MgO | B | 3.54 | | | | | | | |
| M-3-12 | MgO | B | 3.58 | | | | | | | |
| M2N-1-4 | MgO+ 2 w/o NiO | B | 3.47 | | | | | | | |
| M5N-1-3 | MgO+ 2 w/o NiO | B | | | | | | | | |
| M1A-1-5 | MgO-1 w/o $Al_2O_3$ | B | 3.55 | | | | | | | |
| M5A-1-3 | MgO-5 w/o $Al_2O_3$ | B | 3.43 | | | | | | | |
| (Extrusion MgO-21 Insulating Can; Drop Temperature 2080°C, Area Reduction Ratio: 9 to 1) | | | | | | | | | | |
| M-f-13 | MgO | Fusion | 3.58[5] | 3.58[5] | 7-11 to 1 | 101 | 103 | | | |
| M1A-1-14 | MgO+1 w/o $Al_2O_3$ | B | 3.57 | 3.58[5] | 10-13 to 1 | 38 | 40 | | | |
| M5N-1-10 | MgO+5 w/o NiO | B | 3.27 | 3.60[5] | 7-9 to 1 | 22 | | | | |
| M-4-9 | MgO | B | 3.59 | 3.58[5] | 7-9 to 1 | 30 | | | | |
| M-4-11 | MgO | B | 3.53 | 3.58[5] | 11-12 to 1 | 41 | 61 | | | |
| m -1-6 | MgO (Fisher) | Powder | ~1.5 | | 8-11 to 1 | 16 | 27 | | | |
| m -2-1 | MgO (Kanto) | Powder | ~1.5 | 3.48 | 9 to 1 | 10 | | | | |

(1) Billets are listed front to rear.

(2) B refers to vacuum hot pressing procedure or modifications thereof.

(3) Average error estimated at ±0.01 gm/cc.

(4) Average error estimated at ±0.02 gm/cc. Note: Cracking will reduce apparent density.

(5) Approximate theoretical density estimated from transparency.

TABLE IV - BILLET GRAIN SIZE AFTER HEATING FOR EXTRUSION

| Billet | Heated to:[1] | Dia. (in) | Density, gm/cc Before Heating | Density, gm/cc After Heating | Grain Size (microns) | |
|---|---|---|---|---|---|---|
| M-1-8 (LiF) | 2200°C | 1.5 | 3.53 | 3.58 | 163 | |
| M5N-1-1 (LiF) | " | " | 3.27 | | 100 | MgO-7 Extrusion |
| M1A-1-9 (LiF) | " | " | 3.50 | | 400 | |
| M-2-20 | " | " | 3.59 | | 76 | |
| M-3-1 | " | " | 3.54 | | 65 | |
| M-3-2 | " | " | 3.56 | | 50 | |
| M-2-7 | " | " | 3.59 | | 90 | MgO-10 Extrusion |
| M-2-21 | " | " | 3.58 | | 64 | |
| m-1-1 | " | " | 1.5 | | 38 | |
| OP-211 | " | .75 | 3.58 | | Center (98.2)<br>Outside 3000 | |
| M-3-11 | " | 1.0 | 3.59 | | 191 | |
| M-3-22 | " | 1.0 | 3.60 | | 185 | |
| M-3-16 | " | 1.5 | 3.59 | | 507 | MgO-17 Extrusion |
| M-3-20 | " | 1.5 | 3.58 | | 160 | |
| M-3-6 | " | 2.0 | 3.58 | | 162 | |
| m-1-4 | " | .9 | ~1.5 | 3.56 | 54.7 | |

[1] Optical reading at rear of can just before dropping billet.

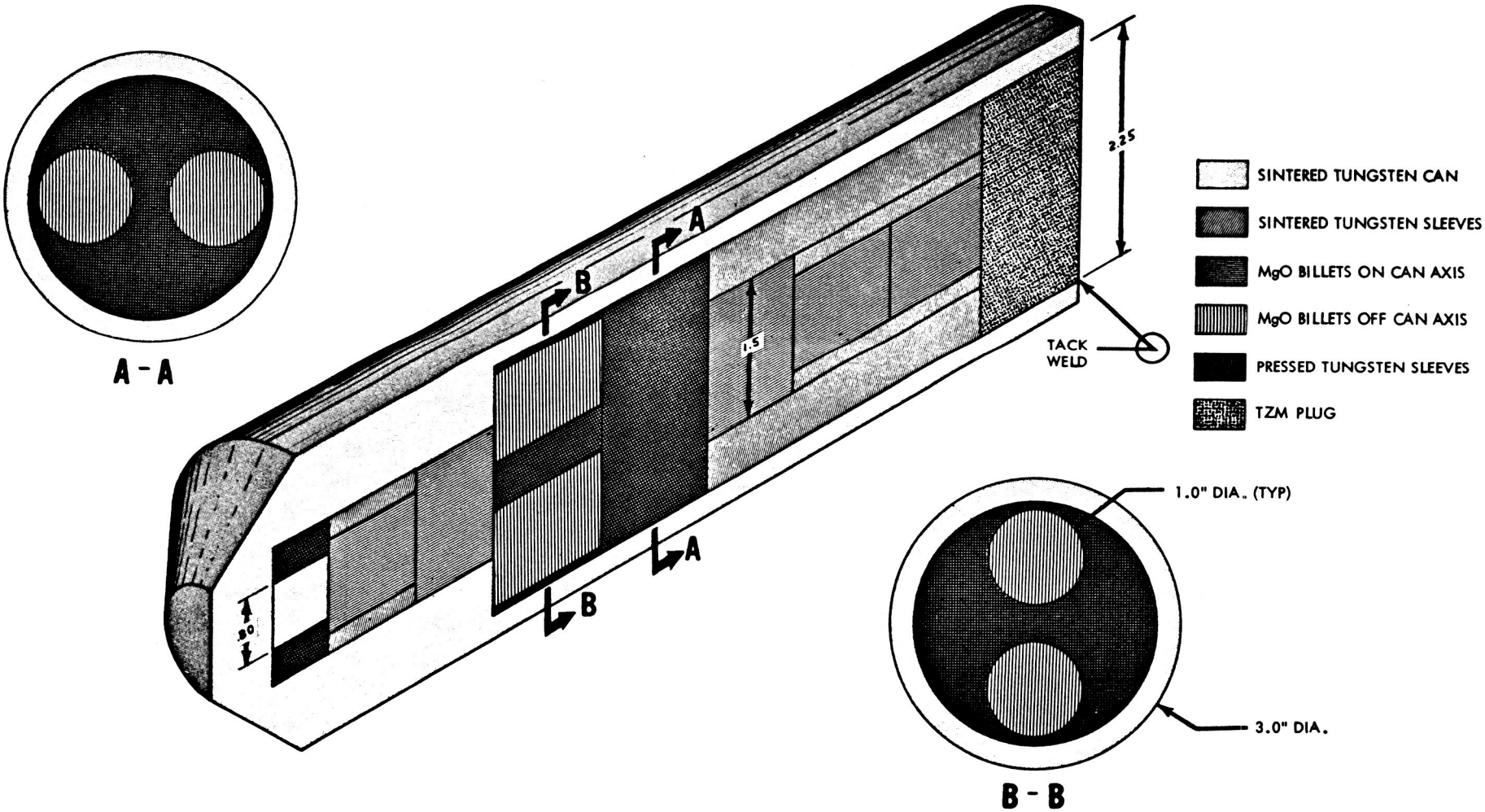


FIGURE 1 OFF-SET BILLET EXTRUSION CONFIGURATION ( MgO -19)

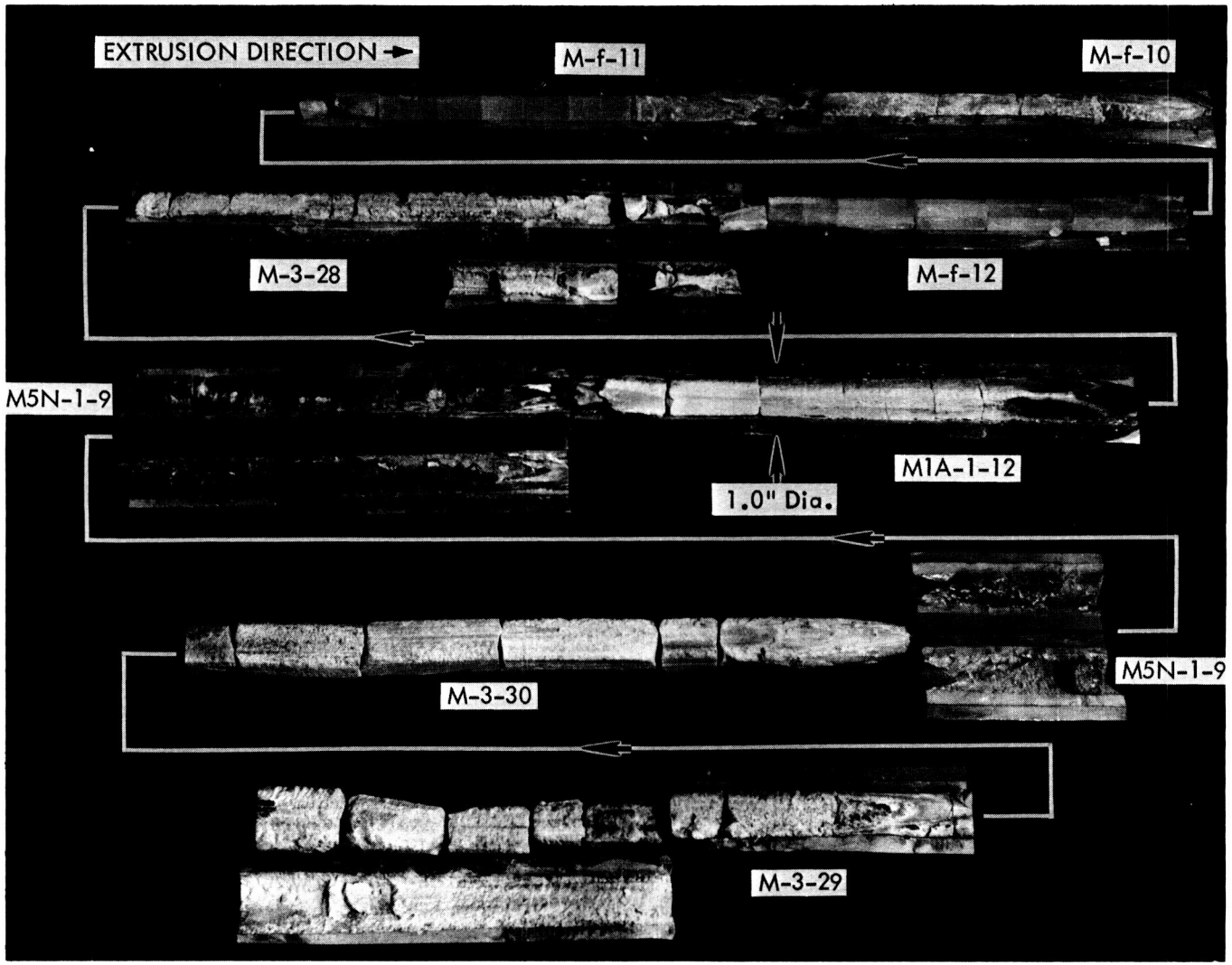


FIGURE 2 EXTRUSION MgO-18. SQUARE BILLETS IN A ROUND CAN, EXTRUDED THROUGH A ROUND DIE.

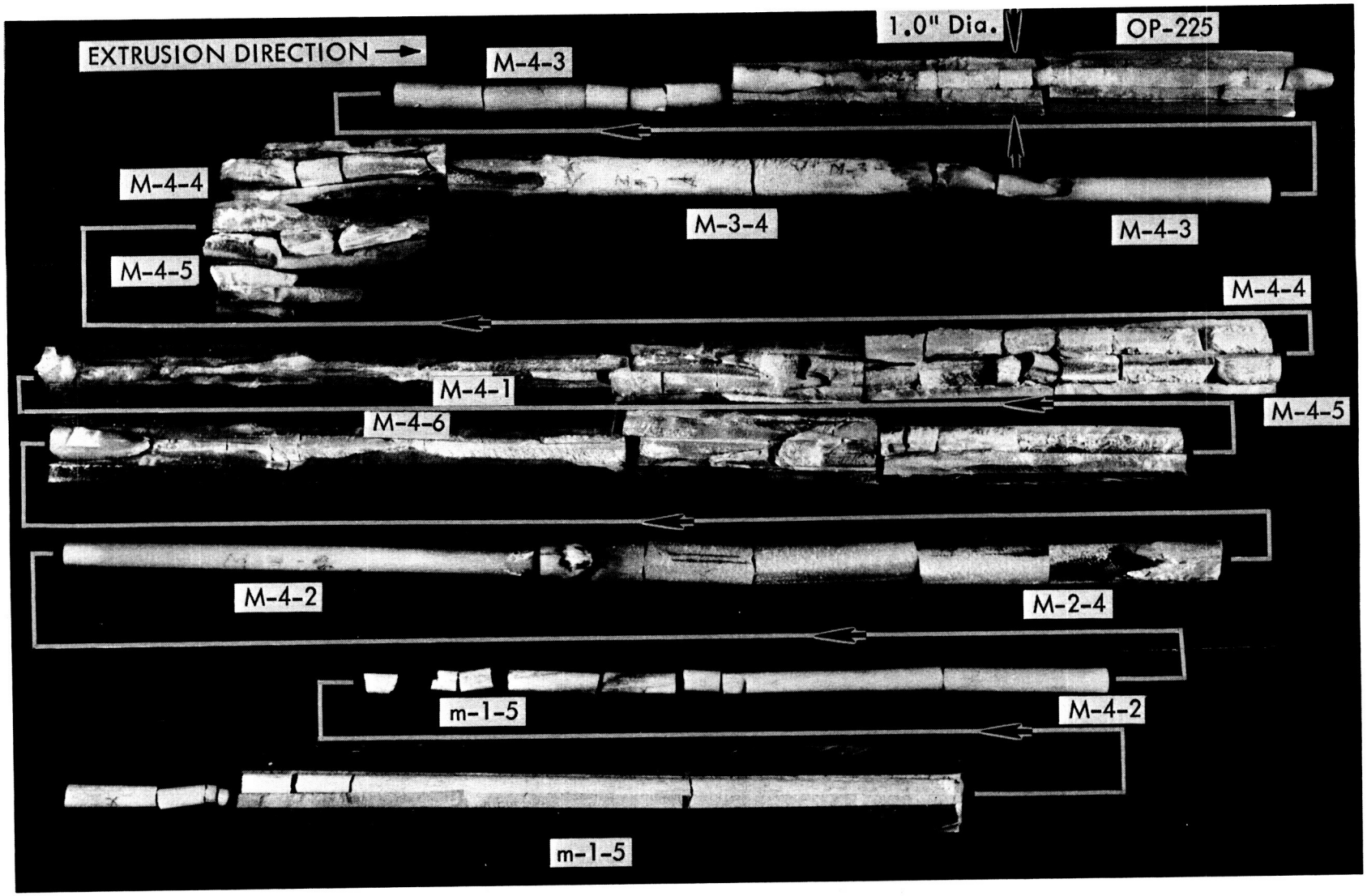


FIGURE 3 EXTRUSION MgO-19. EXTRUSION OF VARIOUS DIAMETER MgO BILLETS, WITH SOME OFF OF THE CAN AXIS, IN A COMMON CAN WITH UNIFORM OUTSIDE DIAMETER.

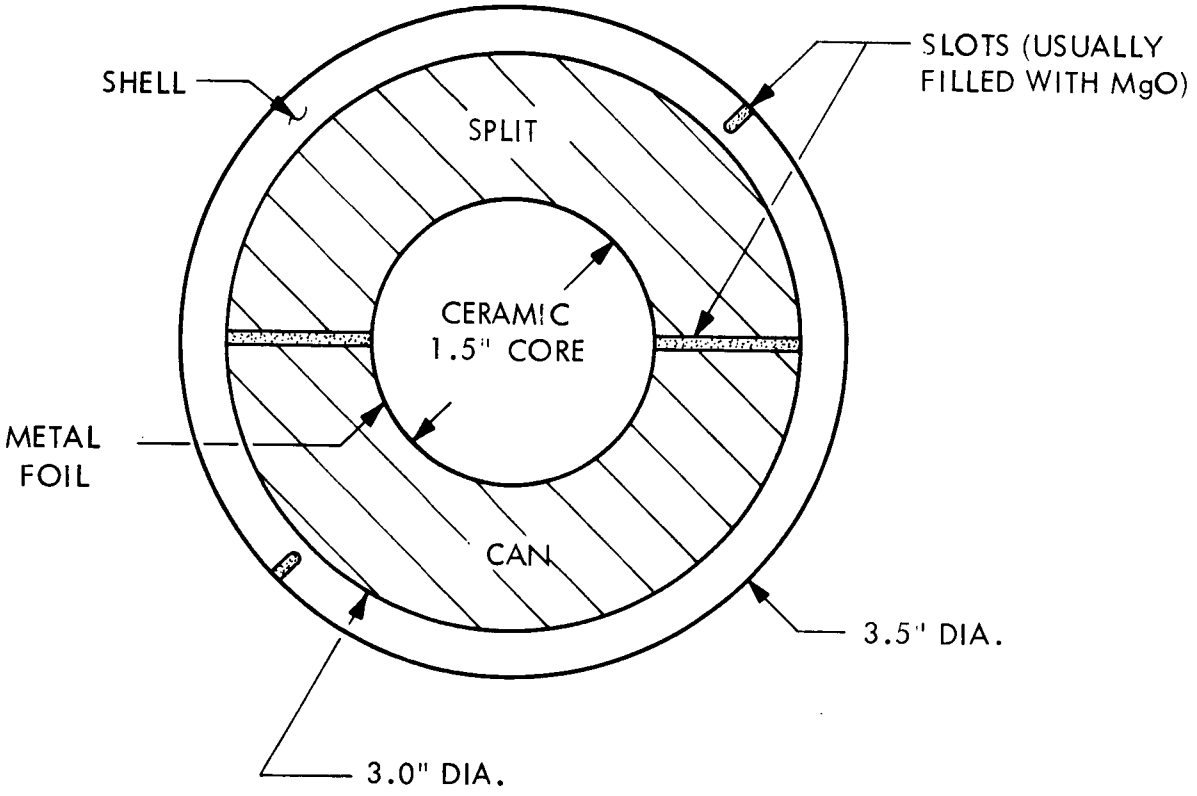


FIGURE 4 SPLIT CAN WITH A SLOTTED SHELL CONFIGURATION

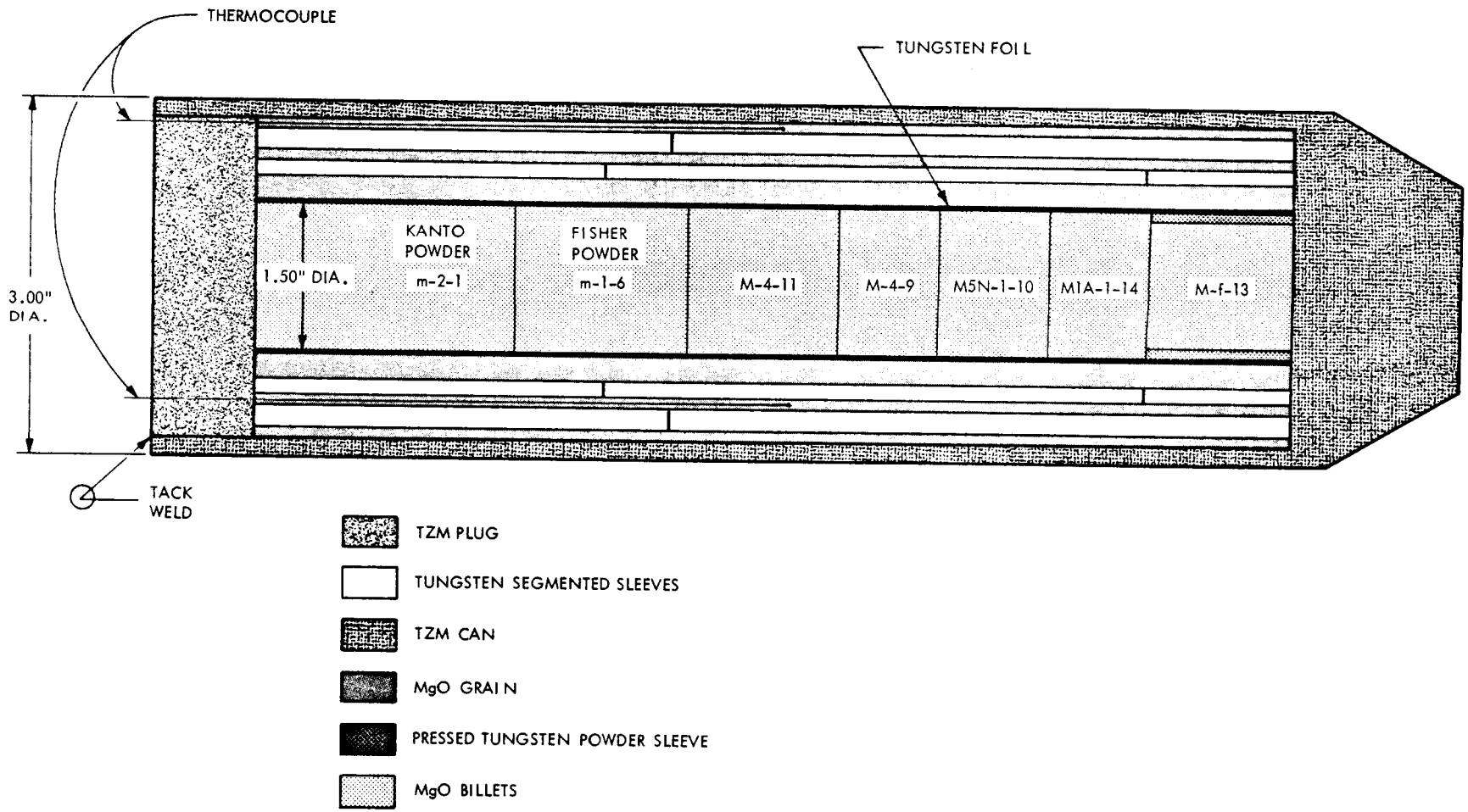


FIGURE 5 INSULATING CAN CONFIGURATION

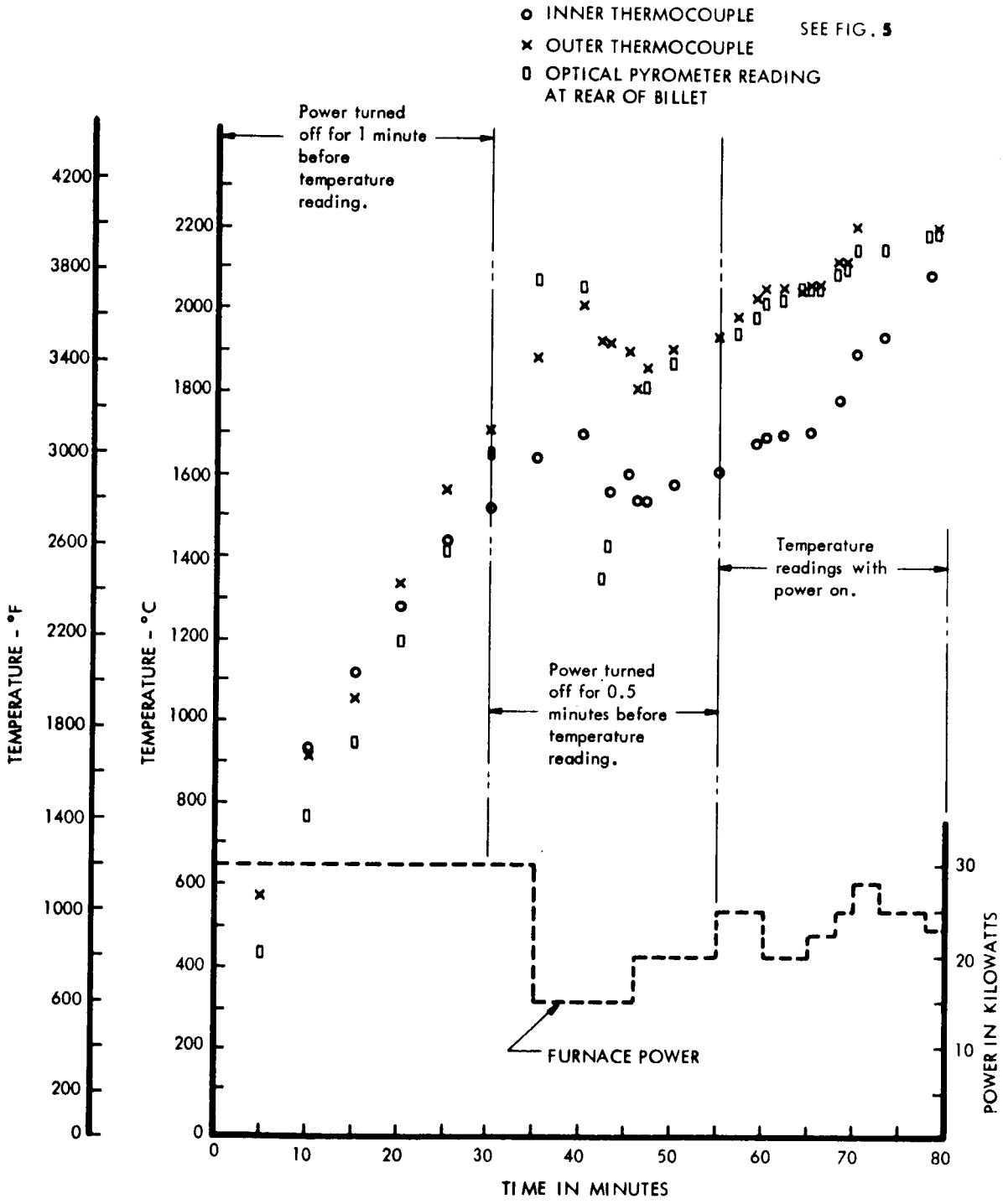


FIGURE 6 TEMPERATURE READINGS FROM THE INSULATING CAN EXTRUSION (MgO-21)

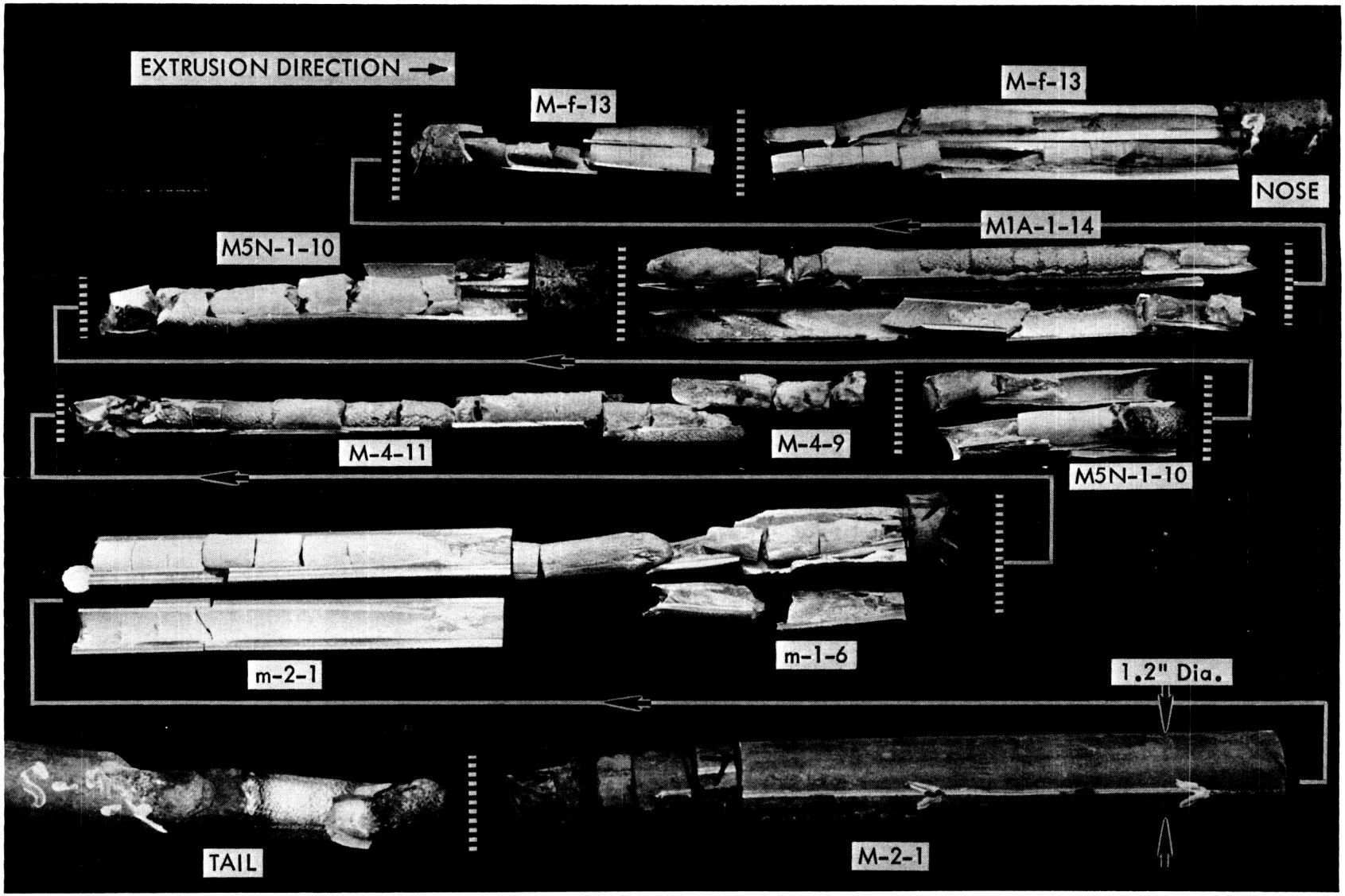


A

FIGURE 7 - EXTRUSION MgO-21 (SELF INSULATING CAN EXTRUSION) NOTE VERTICAL DASHED LINES INDICATING BREAKS IN EXTRUSION A. GENERAL LAYOUT

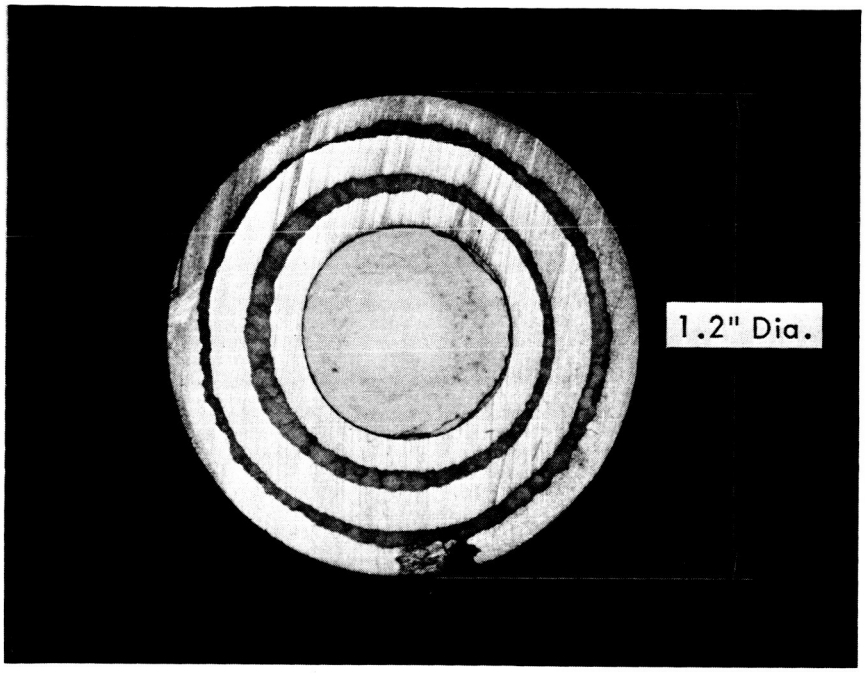


B

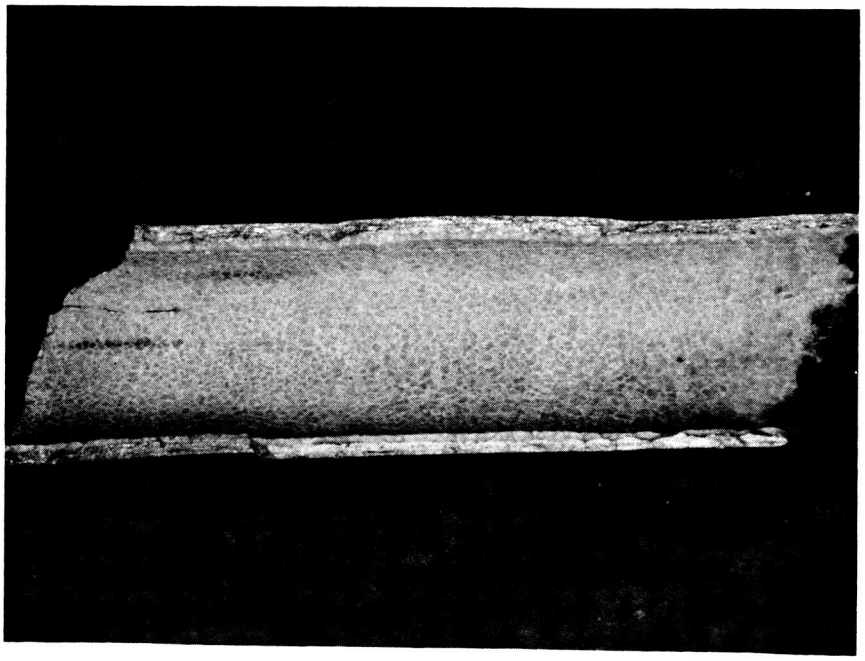

C

FIGURE 7 EXTRUSION MgO-21 (Cont'd). (B) CROSS SECTION, (C) SAMPLE OF TZM SHELL WITH MgO "INSULATING" COATING.

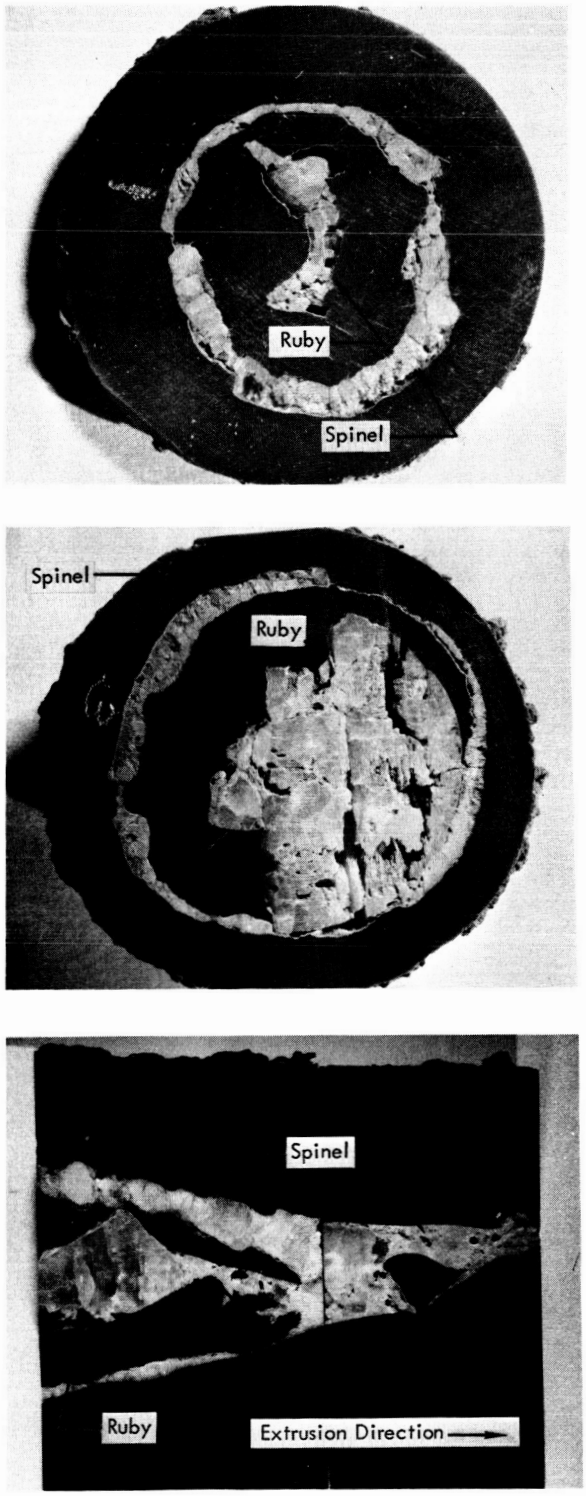


A

B

C

1.2" Dia.

FIGURE 8 EXTRUSION $Al_2O_3$ - 3 SAMPLES. (A) TRANSVERSE CROSS SECTION. (B) SECOND TRANSVERSE CROSS SECTION ABOUT 0.1" IN FRONT OF (A). (C) LONGITUDINAL CROSS SECTION ABOUT 0.1" IN FRONT OF (B). NOTE ANGULAR SHAPE OF RUBY.

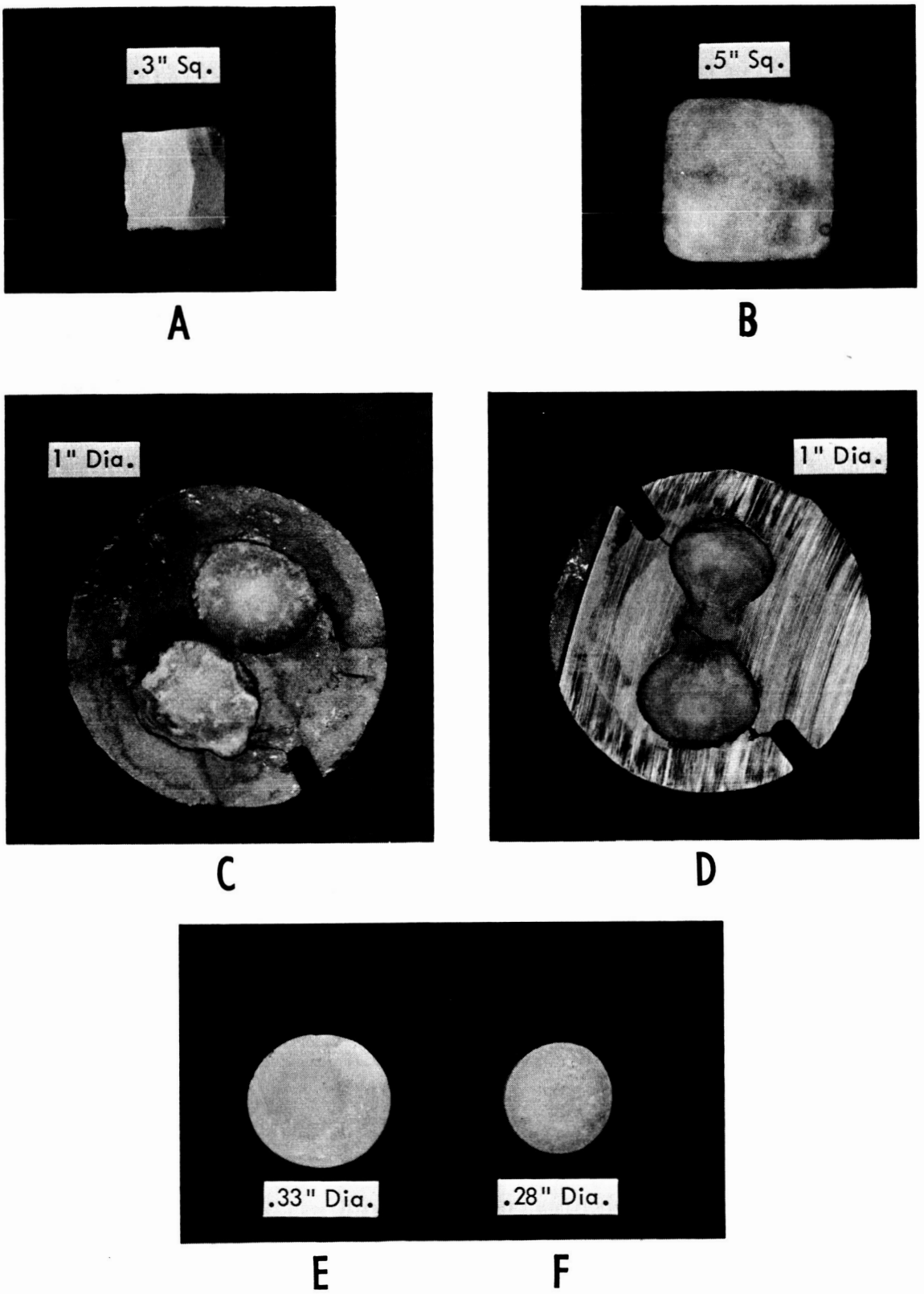


FIGURE 9 SAMPLE EXTRUSION CROSS SECTIONS
(A), (B) M-f-11 and M-3-30 RESPECTIVELY OF EXTRUSION MgO-18.
(C), (D), (E), (F) M-4-4 AND M-4-5, M-4-1 AND M-4-6, M-4-3 AND M-4-2 RESPECTIVELY OF EXTRUSION MgO-19.

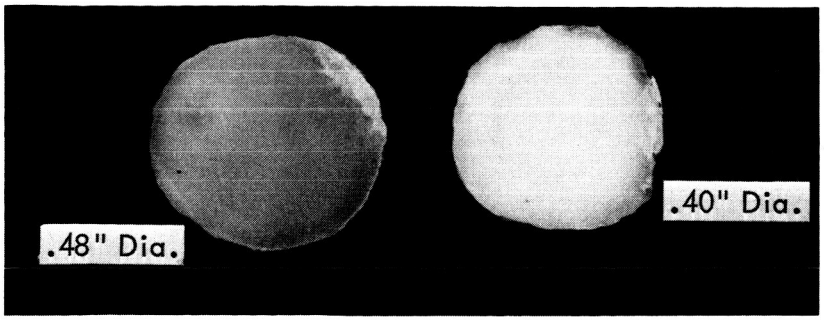


G H

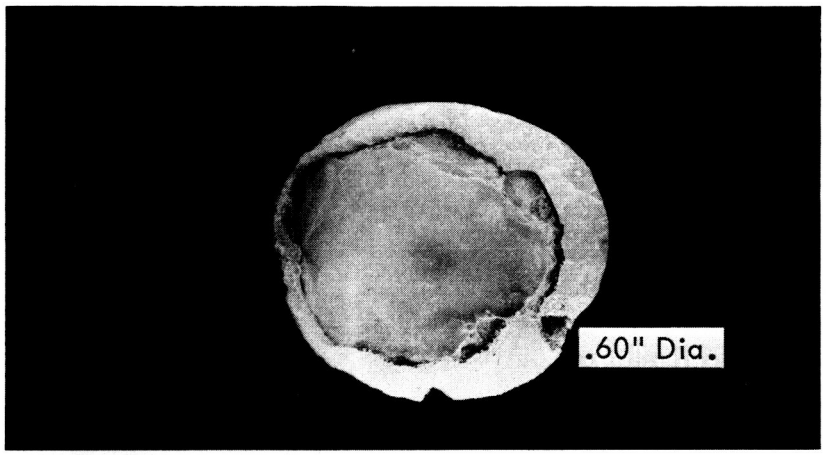


I

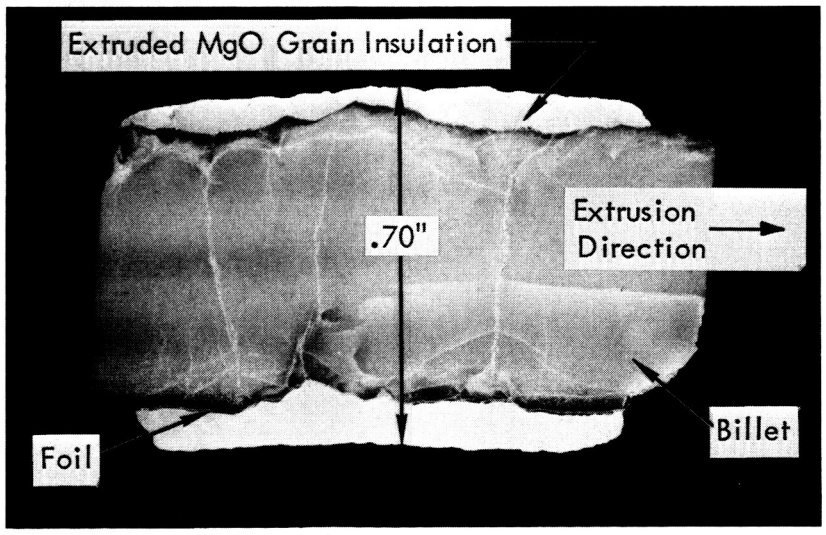


J

FIGURE 9 (Cont'd) SAMPLE EXTRUSION CROSS SECTIONS (G), (H), (I) M1A-1-14, M-4-11 AND M5N-1-10 RESPECTIVELY OF EXTRUSION MgO-21. (J) LONGITUDINAL CROSS SECTION OF M5N-1-10.

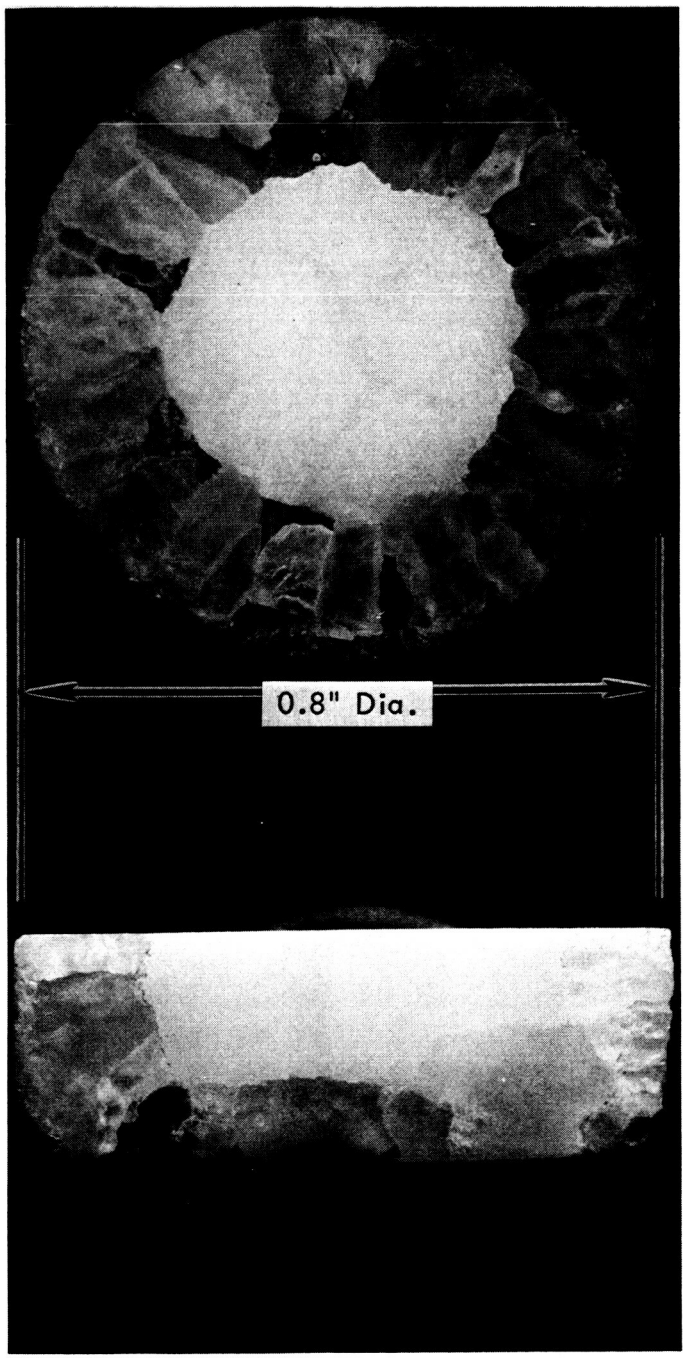


A

B

FIGURE 10 CROSS SECTION OF STALLED JPL HIGH PURITY MgO BILLET (OP-211 FROM M. LEIPOLD OF JPL) (A) CROSS SECTION, (B) FRONT - IN CONTACT WITH TUNGSTEN NOSE.

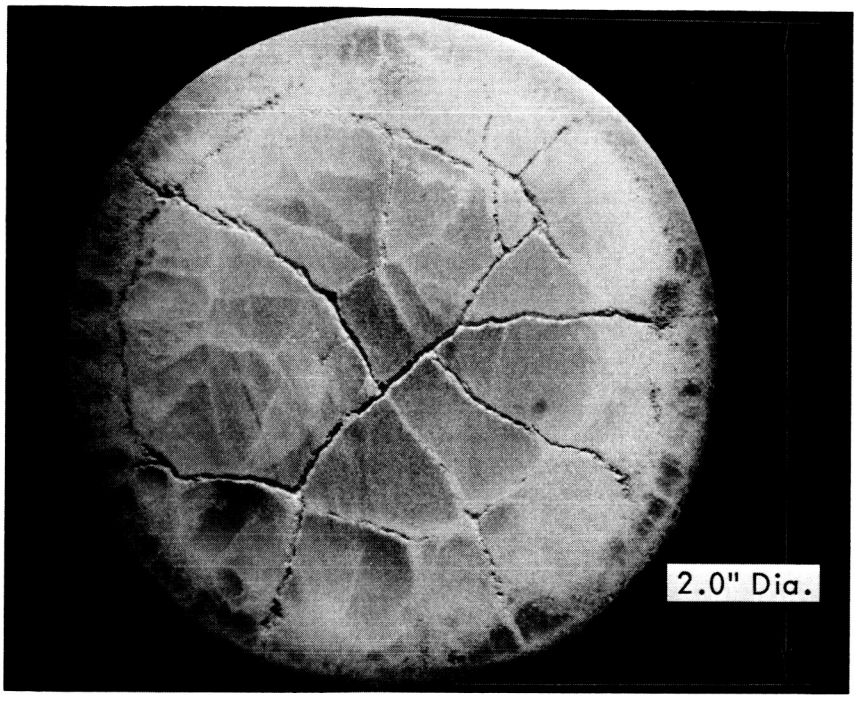


FIGURE 11 CRACKING OF STALLED MgO BILLET

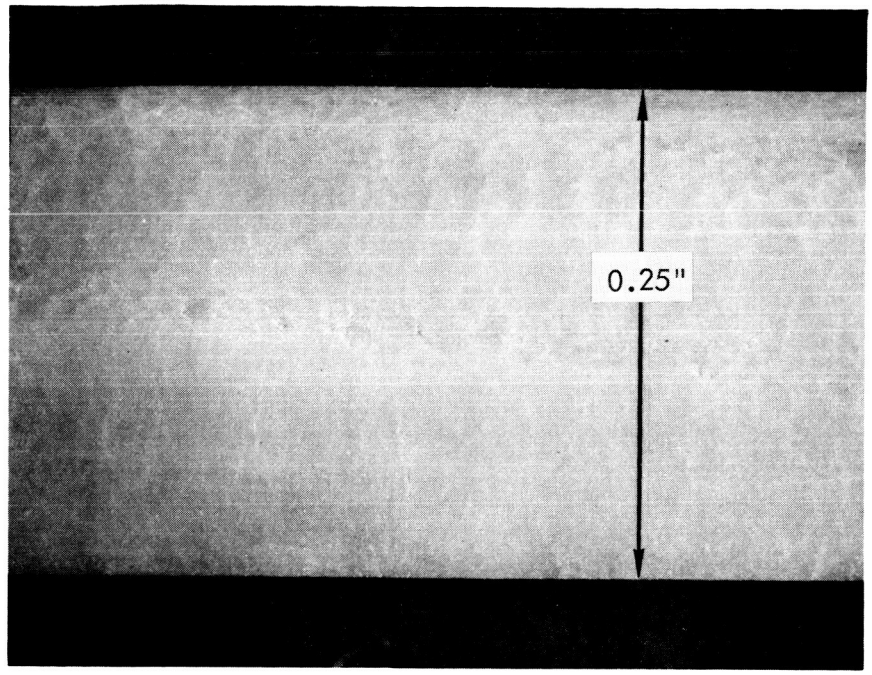


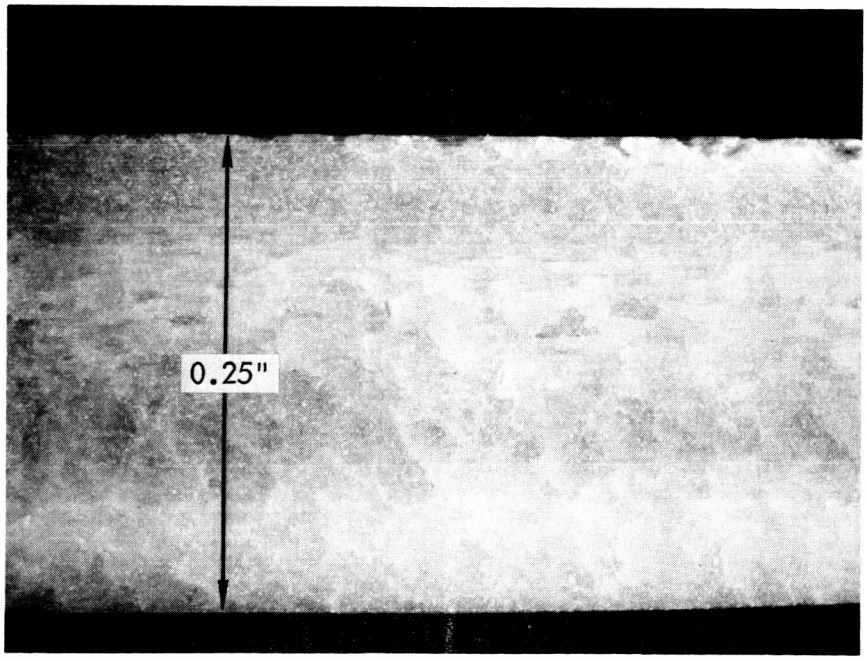


FIGURE 12 HAIR LINE CRACKS IN EXTRUDED MgO

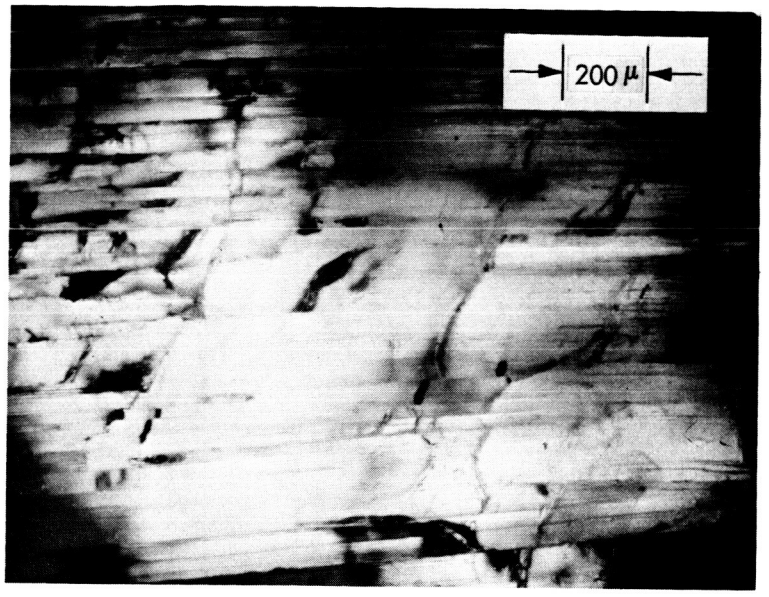


A

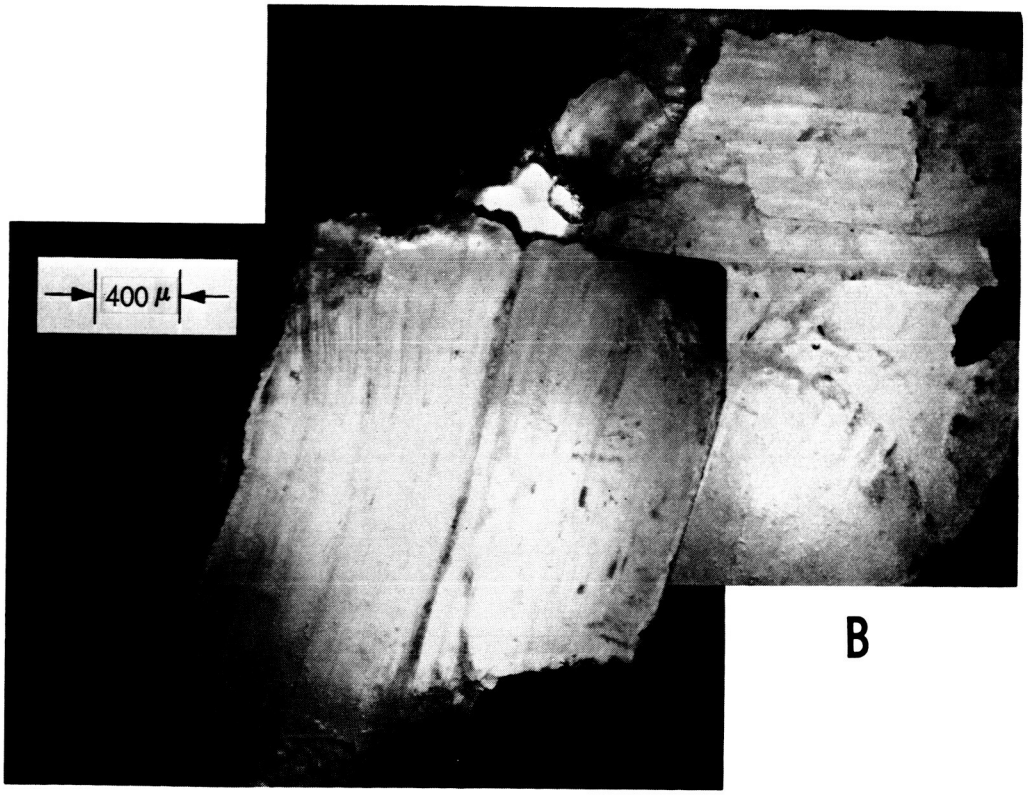


B

FIGURE 13 - EXTRUDED RUBY MICROSTRUCTURE. (A) SAMPLE SECTION. NOTE BENDING OF LAMELLAE AT RIGHT. (B) LOWER MAGNIFICATION. NOTE CHANGES IN LAMELLAE DIRECTIONS.

## APPENDIX 1

## BILLET VACUUM HOT PRESSING PROCEDURE B (WITHOUT LiF)

1. Powder is directly loaded into the die from sealed bottles, without any prior milling unless milling was previously used to mix alloy agents. Pyrolytic graphite spacers are used between the rams and the specimen when graphite dies are used.

2. The powder is cold pressed at 1000 - 2000 psi.

3. The die is placed in the vacuum hot press which is pumped down to a chamber pressure of $10^{-4}$ to $10^{-5}$ torr in about one hour.

4. After at least 2 hours at $10^{-4}$ - $10^{-5}$ torr the die is heated to 1650°F (900°C) in about 30 minutes. Temperatures are measured optically at the approximate center of the side of the die.

5. Starting at 1750°F(950°C) the ram pressure is built up to 5000 psi over a period of about 2 minutes.

6. A temperature of 2400°F(1315°C) is then reached in about 20 minutes, while maintaining the ram pressure at 5000 psi.

7. Pressing conditions of 2400°F and 5000 psi are held for 15 minutes with vacuum chamber pressure averaging about $10^{-2}$torr.

8. The induction heating power is shut off and the ram pressure released over a period of about 1 minute.

9. The die is removed from the vacuum hot press after cooling for two to four hours.

10. The specimen is ejected from the die at a temperature of 750°F(400°C) or less.

## APPENDIX 2

## CALCINING PROCEDURE A

1. Powder is loaded in 99% pure MgO crucibles approximately 3" in diameter x 4" high with 0.1" wall thickness by using the crucible to scoop powder from the container.

2. The crucibles are placed in a metal retort with half of them inverted on top of the remainder. The top crucibles are slotted on the side near their base to allow ready gas escape and good flushing while acting as lids to prevent excess spillage of powder, and possible contamination from the retort metal lid.

3. A thin metal lid is welded on the retort to seal it.

4. Lines are attached to fittings to introduce argon at the bottom in front, and a vacuum line to the top of the retort in the back.

5. The retort is loaded in the furnace and the vacuum and argon valves are set to establish an argon flush at about 10" absolute pressure.

6. The retort is heated at a linear rate to reach 600°C(1110°F) in approximately 5.5 hours. Temperatures are measured by a thermocouple near the center of the retort.

7. After 1 hour at 600°C, the retort is cooled in approximately 1.5 hours, initially in the furnace, then out of the furnace.

8. When the retort is less than 100°C the vacuum valve is closed. When the retort is nearatmospheric pressure, the argon valve is closed, and the retort is flooded with benzene through a third fitting.

9. The thin retort lid is then removed and the powder, covered with benzene, is transferred to jars which are closed for storage.

APPENDIX 3

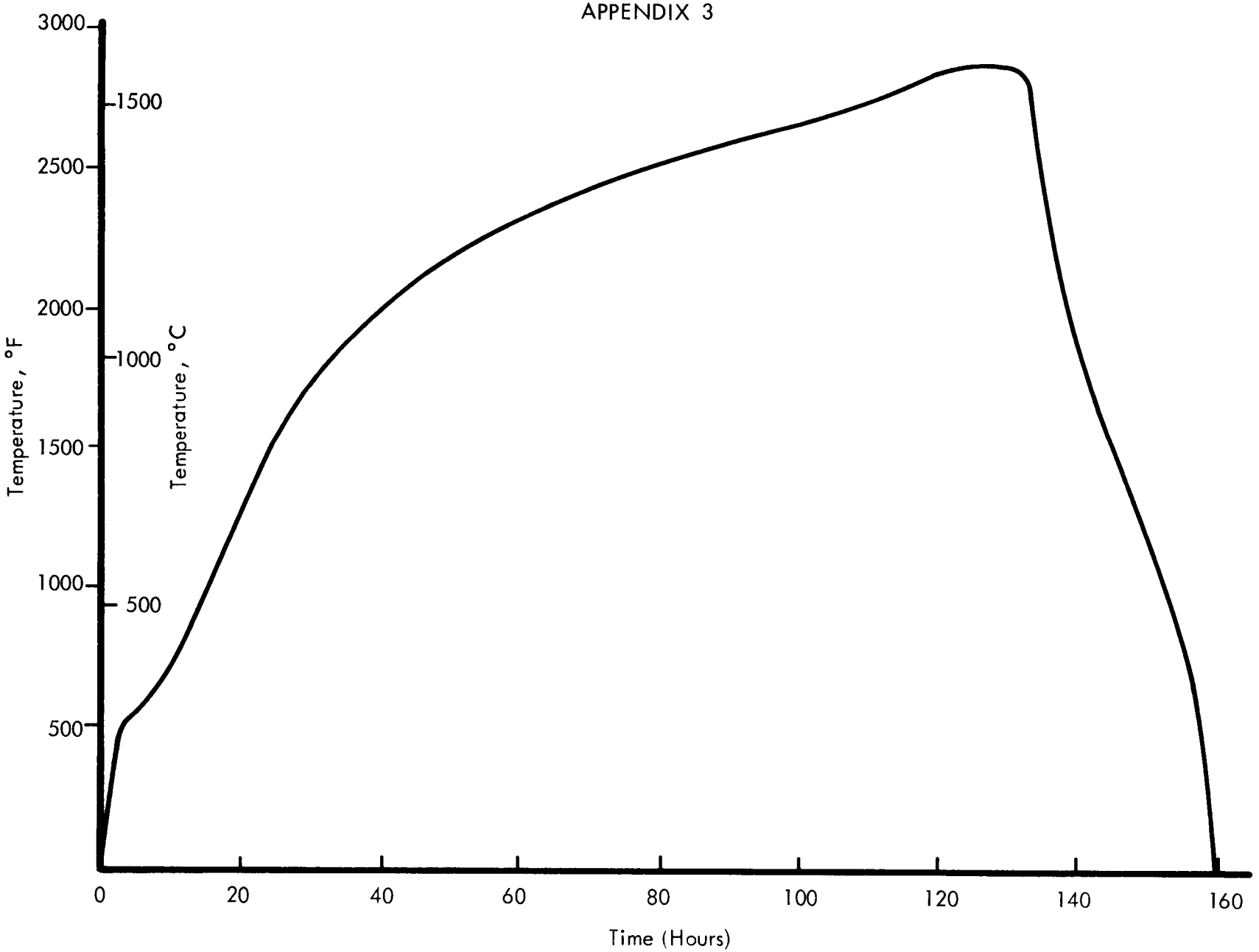


FIRING SCHEDULE A

## APPENDIX 4

## SURFACE WORK HARDENING OF MgO CRYSTALS

Fracture origins of extruded MgO samples prepared by sanding have been reported to occur predominately from the interior rather than the surface of the body in Progress Report 8 (Interim Report II). It was postulated that this was due to work-hardening (probably like that reported by Alden[1]) reducing the chance of slip and associated crack nucleation in surface grains. Several examples of sanded surface grains with high dislocation or slip band densities along the edge were shown. Subsequently in Progress Report 10, it was reported that removal of the surface of sanded specimens by chemical polishing returned the fracture origin to the surface. Also, fracture origins occurred with increasing frequency at the surface of sanded specimens after annealing at increasing temperatures.

A final test of this postulate appeared to be examination for this phenomena in single crystals. Comparison of MgO crystal fracture surfaces after cleavage, chemical polishing, or sanding clearly showed a high density of slip bands along the surface of the latter (Figure 1). Comparison of softer Semi-Elements MgO crystals (apparently due to higher purity) with Norton MgO crystals indicates a greater depth of such hardening in the softer material (Figure 2).

These single crystal observations provide additional support for the postulated surface work hardening of polycrystalline MgO. A detailed study of any yield stress and fracture origin effects of such dense surface slip in MgO crystals might also be of value, but is not felt to be in the scope of this program. However, it is noted that Scott[2] attributed increased brittleness in LiF crystals prepared by cutting to a work hardened layer rather than surface defects because:

(1) Fracture stress of cut specimens remained high (flaws would be expected to give a few relatively weak specimens).

(2) Large cracks were not altered by annealing which in all cases restored ductility to cut specimens.

(3) There was an obvious interference to dislocation motion as evidenced by the small amount of plastic flow which occurred at high stresses in cut specimens.

Thus, it is quite possible that a very slight hardening of surface grains could lead to fracture in the interior grains as reported.

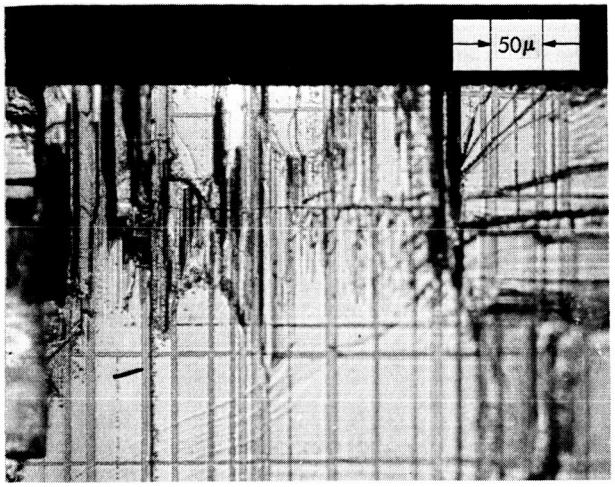


A

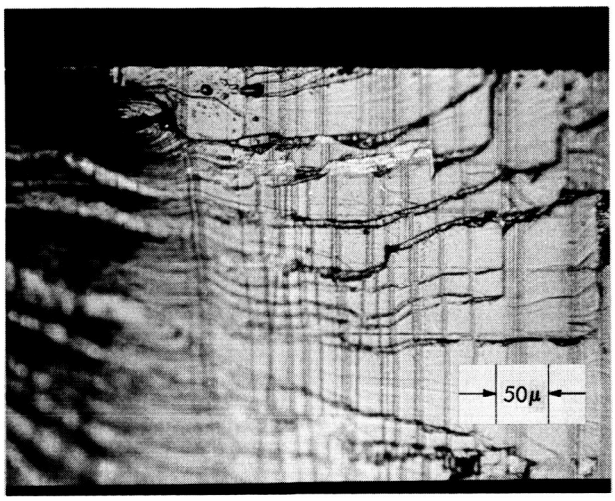


B

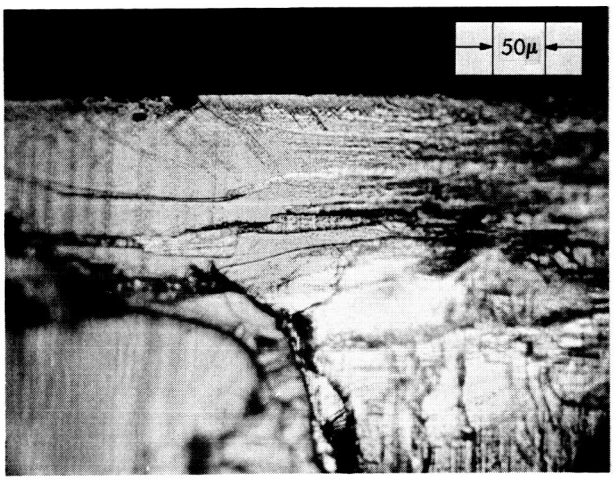


C

FIGURE 1 SURFACE WORK HARDENING IN MgO CRYSTALS.
Etched (approximately 5 seconds in boiling chromic acid) ⟨100⟩ fracture surfaces of Norton MgO crystals after: A) Cleavage, B) Chemical Polishing (5 minutes in phosphoric acid), C) Dry sanding on 400 grit SiC paper - note high slip band density along edge not found in A or B.

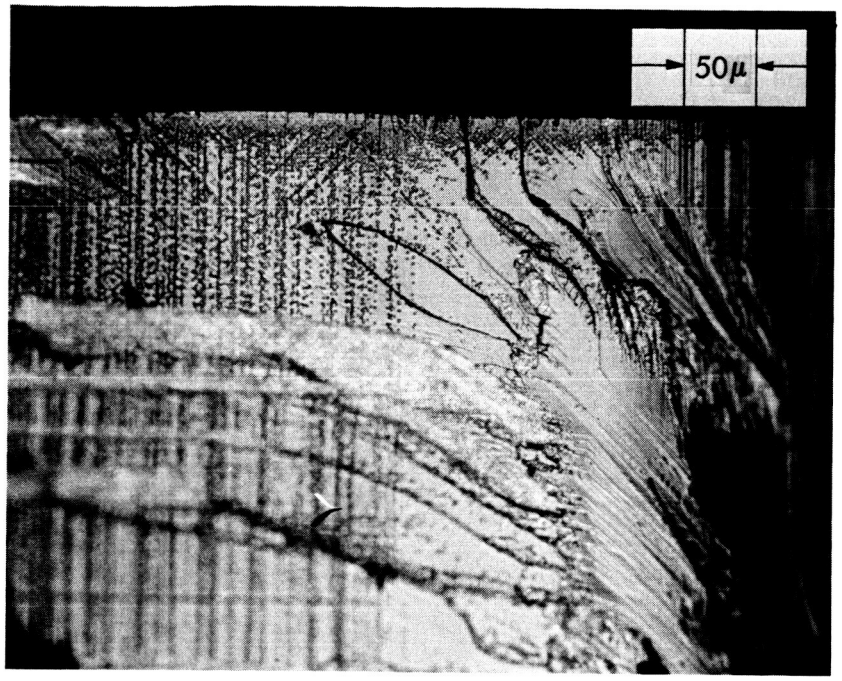


A

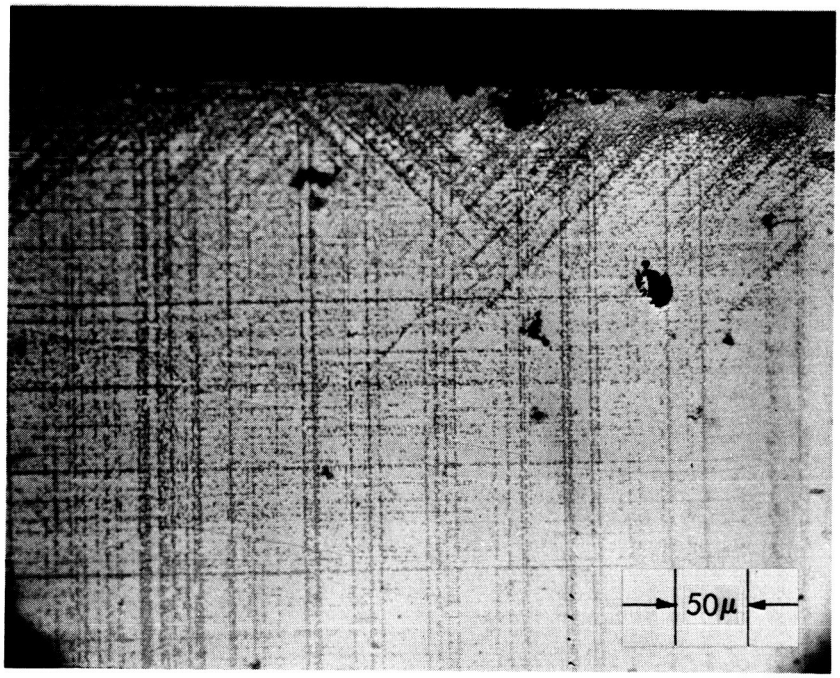


B

FIGURE 2 INCREASED SURFACE WORK HARDENING IN SOFTER MgO CRYSTALS. Etched (approximately 5 seconds in boiling chromic acid) ⟨100⟩ fracture surfaces of A) Norton MgO crystal tested as sanded; Yield stress: $18.8 \times 10^3$ psi; B) Semi-Elements intermediate (improved purity) grade MgO crystal tested as sanded; Yield stress: $10.7 \times 10^3$ psi.

## REFERENCES


1a. T. H. Alden, "High-Strength Magnesium Oxide", Appl. Phy. Letters (6) pp. 107-08, March 15, 1963.

1b. T. H. Alden, "The Strain Hardeningof Magnesium Oxide Single Crystals", Trans. Met. Soc. AIME 227, 1963, October 1963.

2. W. D. Scott, "Deformation and Fracture of Polycrystalline LiF", Ph.D. Thesis, University of California at Berkeley, September 1962 (Lawrence Radiation Lab Report UCRL-10435).